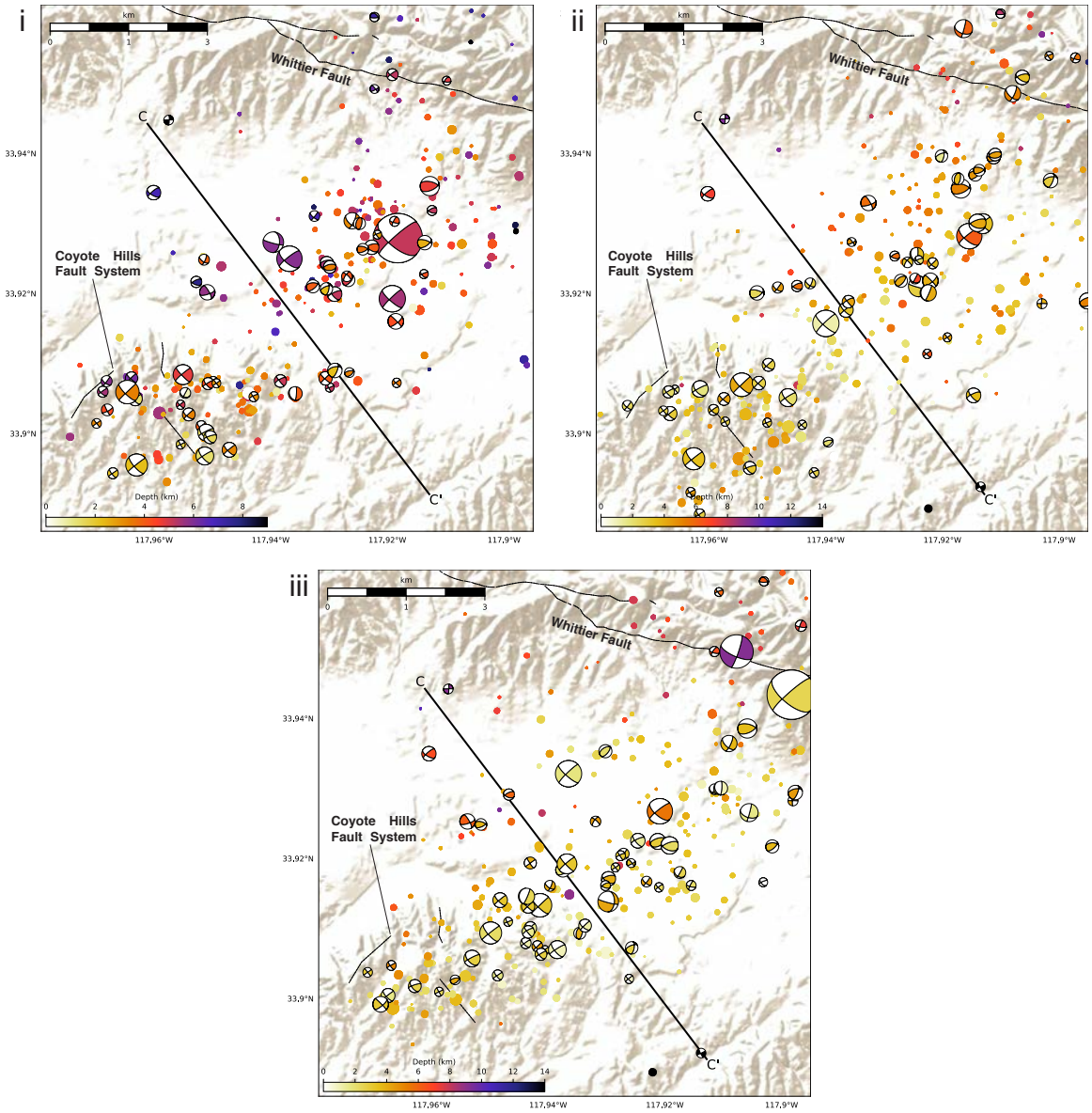

Figure 61: Relocated maps of the La Habra Sequence using a 0.2 RMS differential travel time residual and the three different velocity models. Figure 61-i shows the relocation results using the IASP91 velocity model. Figure 61-ii display the relocation results using the smoothed southern California velocity model. Figure 61-iii are the relocation results from the LA Basin velocity model. Symbols as in Figure 55.

The events making up the La Habra Sequence relocated into two distinct sets of earthquakes (Figure 61-i) using the IASP91 velocity model. One of these is centered around the Coyote Hills Fault System, while the other, larger, one is located approximately equidistant from the Whittier Fault and the Coyote Hills Fault System. The events centered around the Coyote Hills Fault System consist predominantly of strike-slip

events at relatively shallow depths, whereas the center set of events is composed of a mixture of strike-slip and reverse, smaller magnitude, events at greater depths (Figure 61-i). This central cluster contains the 2014 La Habra Mainshock.

In cross-section, the events appear to be consolidated along a near-vertical or steeply dipping relatively shallow feature (Figure 62-i). These events are not highly consolidated, however. The depths of these relocated events are very shallow, with the maximum depth less than 10 km, while the majority of the events occurred at depths less than 5 km. The largest event in this sequence, the 2014 La Habra Earthquake, occurs at approximately 5 km depth.

The relocations produced by the smoothed southern California velocity model show similar clustering as the IASP91 model relocations (Figure 61-ii). However, both relocations present a less consolidated form than the IASP91 velocity model. The clustering around the Coyote Hills Fault System consist mainly of strike-slip motions, while, based on the focal mechanisms presented in Figure 61-ii, the central cluster contains a mixture of reverse and strike-slip motion events (Figure 61-ii). While the majority of the large events within the La Habra Sequence were relocated within either of these two clusters, for the IASP91 model relocations the locations show more variation for the larger events. The smoothed southern California model relocations do not include the 2014 La Habra Earthquake. The cross section of these relocations confirm the loose consolidation previously discussed, in addition to the lack of a noticeable planar dipping fault structure (Figure 62-ii).

Of the three relocation results of the La Habra Sequence shown, visually those for the LA Basin velocity model show the tightest distribution (Figure 61-iii). Rather than two separate series of events making up the sequence as seen in the other two model relocations, these results show a single trend of events spanning from the Coyote Hills Fault System to the Whittier Fault. The largest of these events, the 2014 La Habra mainshock, is situated along the northeastern edge of the Sequence, straddling the

Whittier Fault (Figure 61-iii). This location along the sequence in association with the northeast-southwest oriented nodal plane of the focal mechanism indicates that this sequence likely occurred on a left-lateral fault. As seen in the previous two model relocation results, earthquakes in close proximity to the Coyote Hills Fault System exhibit primarily a strike-slip mechanism, while the reverse motion events are situated towards the northeast (Figure 61-iii).

The cross section of these model relocations confirm the previous statements that these events have consolidated into a tighter trend of events (Figure 62-iii). These locations, similar to the IASP91 model relocations, are centered around a steeply-dipping structure towards the northeast. The majority of the event locations along this structure are located at depths greater than 5 km.

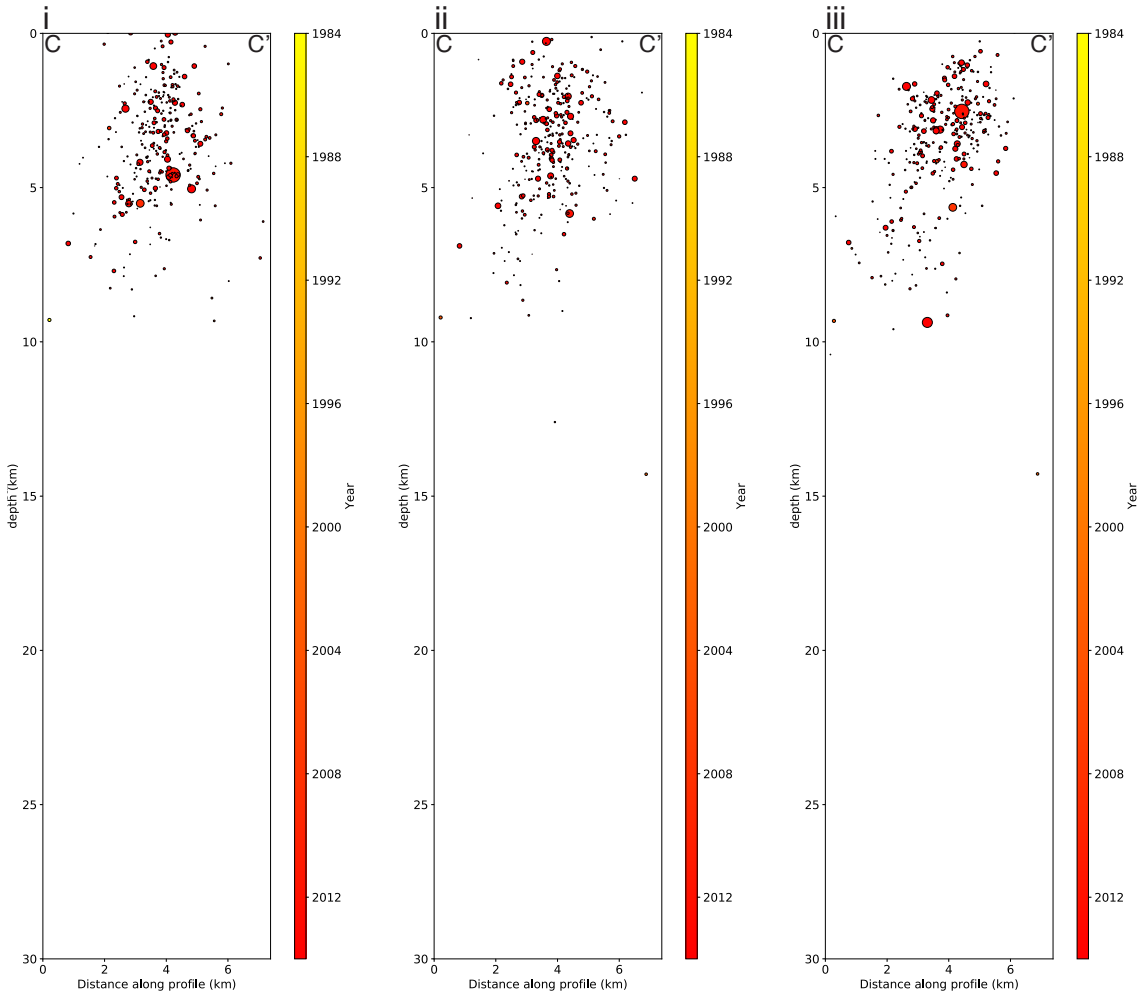

Figure 62: Cross sections illustrating each of the relocations of the La Habra Sequence using a 0.2 RMS differential travel time residual and the three different velocity models used. Figure 62-i shows the relocation results using the IASP91 velocity model. Figure 62-ii display the relocation results using the smoothed southern California velocity model. Figure 62-iii are the relocation results from the LA Basin velocity model.

Unlike the Yorba Linda and Chino Hills Sequences, the La Habra Sequence has high relocation errors for all velocity models. The smoothed southern California velocity model possesses both the lowest average horizontal and vertical errors, while the LA Basin velocity model relocations have the highest average errors (Figure 63). With the high errors among all relocation results, it is difficult to have a high level of confidence in the accuracy of these relocations.

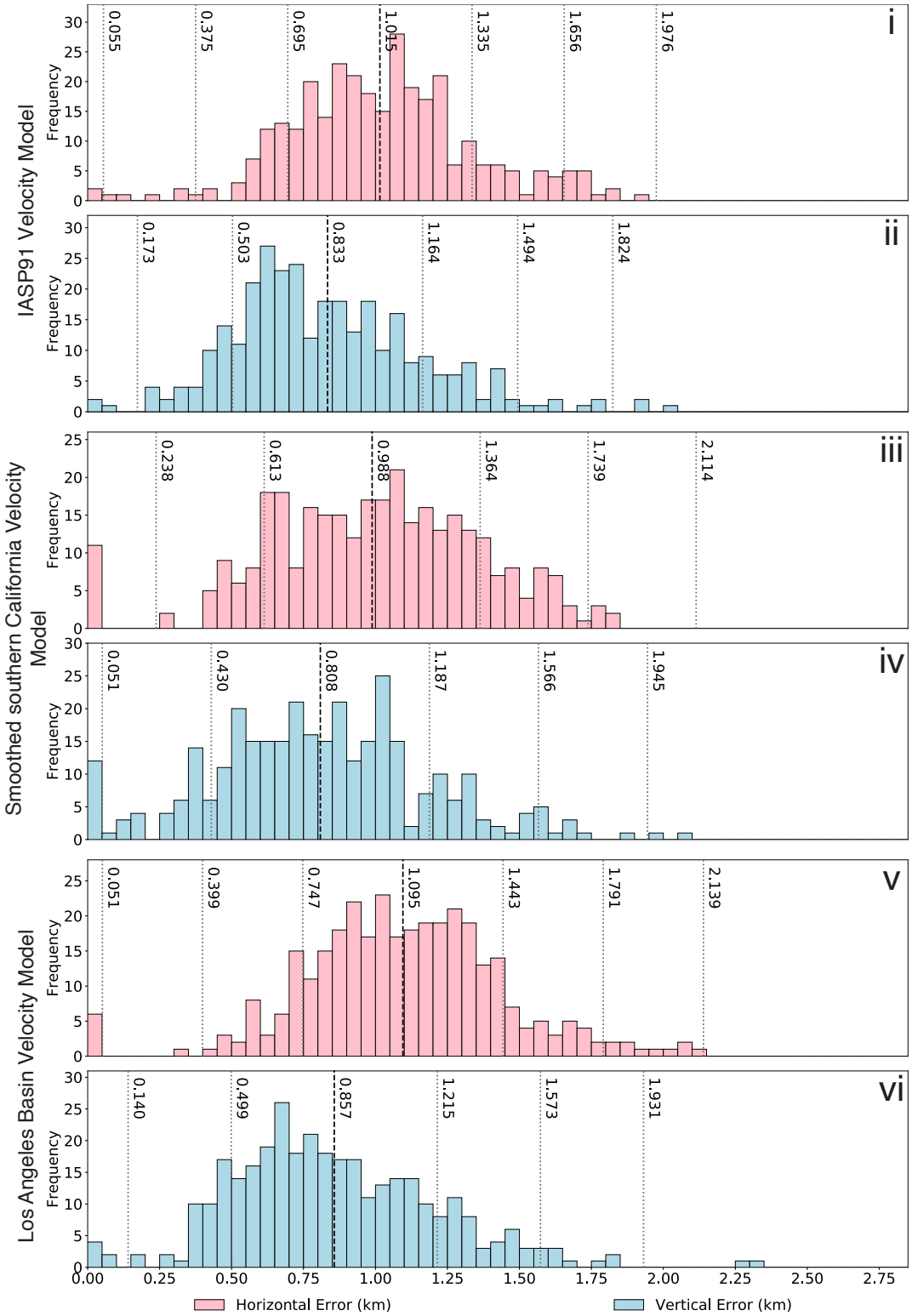

Figure 63: Histograms of the horizontal and vertical errors of the relocations for each velocity model of the La Habra Sequence, respectively. The black, dashed line indicates the average location error while the gray, dotted lines denote the standard deviations. Figure 63-i and 63-ii represent the IASP91 velocity model. Figure 63-iii and 63-iv represent the smoothed southern California velocity model. Figure 63-v and 63-vi represent Whittier Narrows velocity model.

For the La Habra sequence, the LA Basin velocity model appear to be the logical velocity model to use for relocation. This is because nearly all events making up the La Habra Sequence are contained within the LA Basin. However, it is difficult to ascertain which of the relocations is the optimal one. The LA Basin velocity model resulted in the successful relocation of most earthquakes and is visually the most appealing, in that it produced what appears to be a consolidation of earthquakes along a steeply dipping fault, confirming the hypothesis of a proposed fault within the area. However, the horizontal and vertical errors associated with these relocated events are among the highest between the three models. The smoothed southern California velocity model produced the second highest events relocated and has the lowest average errors overall, despite all three sets of errors for each respective model being high. However, visually, this model produced relocations that were poorly constrained onto a single fault structure of any dip orientation, rather producing events that were all relatively at the same depth within what appears to be a circular cluster. The IASP91 velocity model relocations are considered less ideal in that it resulted in two distinct assemblages of events within the sequence and relocated the lowest number of earthquakes, while falling in between the highest and lowest horizontal and vertical average errors.

A publication regarding the La Habra Sequence states that the La Habra Mainshock and aftershock sequence occurred on a left-lateral strike-slip fault that has a steep dip towards the northeast (Donnellan et al., 2015). While all of our relocation results do portray a linear trend extending from the Whittier Fault towards the Coyote Hills Fault System, only the IASP91 and LA Basin velocity model relocation results indicate a steeply dipping structure based on the hypocenters of the relocations (Figure 62). The LA Basin velocity model relocations do result in a distribution of events that is more similar to a dipping planar structure than the IASP91 velocity model relocations. However, the location errors of these results imply that these relocations are not highly accurate and we do not have a high level of confidence in the presence of this dipping structure in these relocations.

3.2 Results for 0.6 RMS Differential Travel Time Residual

In this section we will briefly describe our results for a 0.6 RMS differential time residual, and compare and contrast these results with those from the previous section for the 0.2 residual. As with the previous table for the 0.2 RMS differential travel time residual, Table 2 shows the relocation statistics using a 0.6 RMS differential travel time residual parameter for all velocity models. As seen in the table, the increase in the RMS differential travel time residual from 0.2 to 0.6 does not significantly increase the number of relocated events (Table 2, Table 3).

The LA Basin velocity model relocation results have the highest number of relocated events (Table 2). Unlike the results for the LA Basin velocity model with a 0.2 RMS differential travel time residual, these relocation results have a higher number of clusters with more than eight events. In addition, this velocity model also does not have the greatest number of event pairs used nor does it use the highest number of P-wave differential arrival times. It does, however use the greatest number of S-wave times.

Table 3: Table depicting the various relocation statistics of the results produced by the GrowClust algorithm for the three different velocity models. ”SoCal” represents the smoothed southern California velocity model and ”LAB” represents the LA Basin velocity model.

Velocity Model	Total events	Relocated Events	Clusters with ≥ 8 events	Relocated events within clusters	Input event pairs	Event pairs used	Xcor data (P-wave)	Xcor data (S-wave)
IASP91	4434	2181	42	1818	2396533	121019	325628	457736
SoCal	4434	2186	46	1872	2396533	97160	278611	408696
LAB	4434	2225	45	1873	2396533	114533	316654	457859

3.2.1 IASP91 Velocity Model Relocation Results

Out of the 4434 catalog events, the GrowClust algorithm managed to successfully relocate 2181 events under a 0.6 RMS differential travel time residual and using the IASP91 velocity model (Table 3). Original locations and relocated locations of every event relocated with respect to depth using this velocity model and RMS differential travel time residual can be viewed in Appendix C: Figure 109 and Appendix D: Figure 112, respectively.

Figure 64 displays a histogram of how far these events were relocated. These relocated events have a wider distribution of relocated distance, as well as a higher average relocation distance compared to the previous results for a 0.2 RMS differential travel time residual parameter. Figure 65 plots these relocated distances on a map of the research area. In the 0.6 RMS IASP91 velocity model relocation results, the Yorba Linda and Chino Hills Sequences were all relocated by smaller distances compared to the 0.2 RMS relocations results for the same velocity model (Figure 65). Similarly to the previous relocation results, distances for the La Habra Sequence are more mixed.

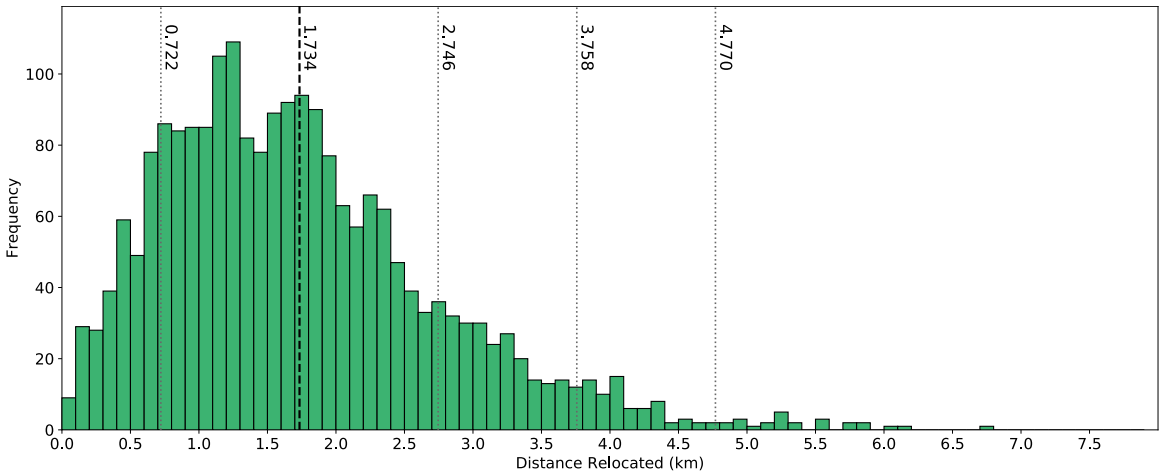

Figure 64: Histogram showing the frequency of events relocated to their new locations using the IASP91 velocity model under a 0.6 RMS differential travel time residual parameter as a function of distance between the original and relocated event location. Labels and lines as in Figure 29.

Comparing the event consolidation of the 0.2 RMS IASP91 velocity model relocation results and the 0.6 RMS IASP91 velocity model relocation results shows that the Yorba

Linda and Chino Hills Sequences for the 0.6 RMS relocations appear to be more scattered (Figure 65). The La Habra Sequence as well as the many clusters situated throughout the area appear to be more tightly constrained than what is seen with the 0.2 RMS IASP91 velocity model relocations.

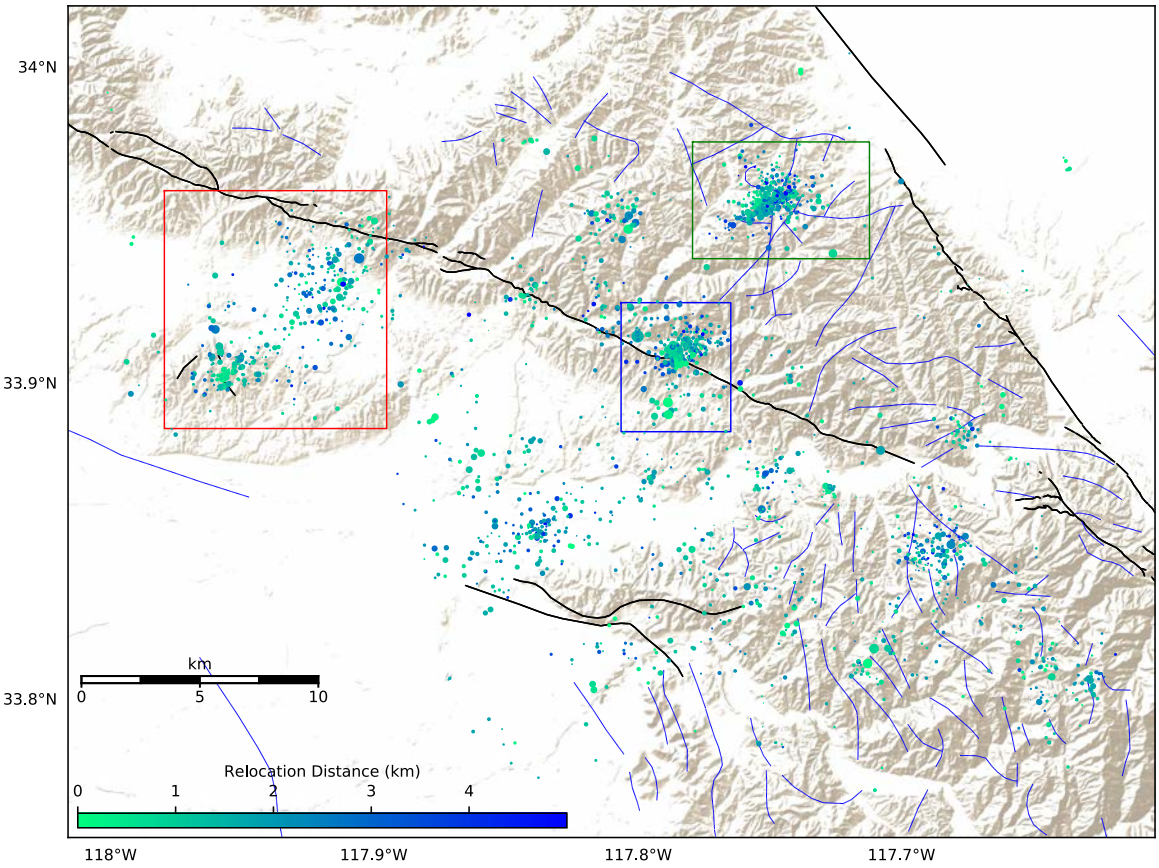

Figure 65: Map of relocated events color coded by the distance each event was relocated compared to its original location, using the IASP91 velocity model with a 0.6 RMS differential travel time residual. The blue box outlines the Yorba Linda Sequence (Figure 94-i), the green box denotes the location of the Chino Hills Sequence (Figure 97-i), and the red box represents the La Habra Sequence (Figure 100-i).

The GrowClust algorithm combined the 2181 events into 295 clusters. Of these 295 clusters, only 42 consisted of more than eight events (Table 3). This is significantly less than the 58 clusters created for the 0.2 RMS IASP91 velocity model relocation results. These clusters are plotted in Figure 66 and their respective centroid locations and number identification are shown in Figure 67. The smaller clusters are dramatically more consolidated that those of all prior relocation results, particularly clusters located

southwest from the Yorba Linda Sequence.

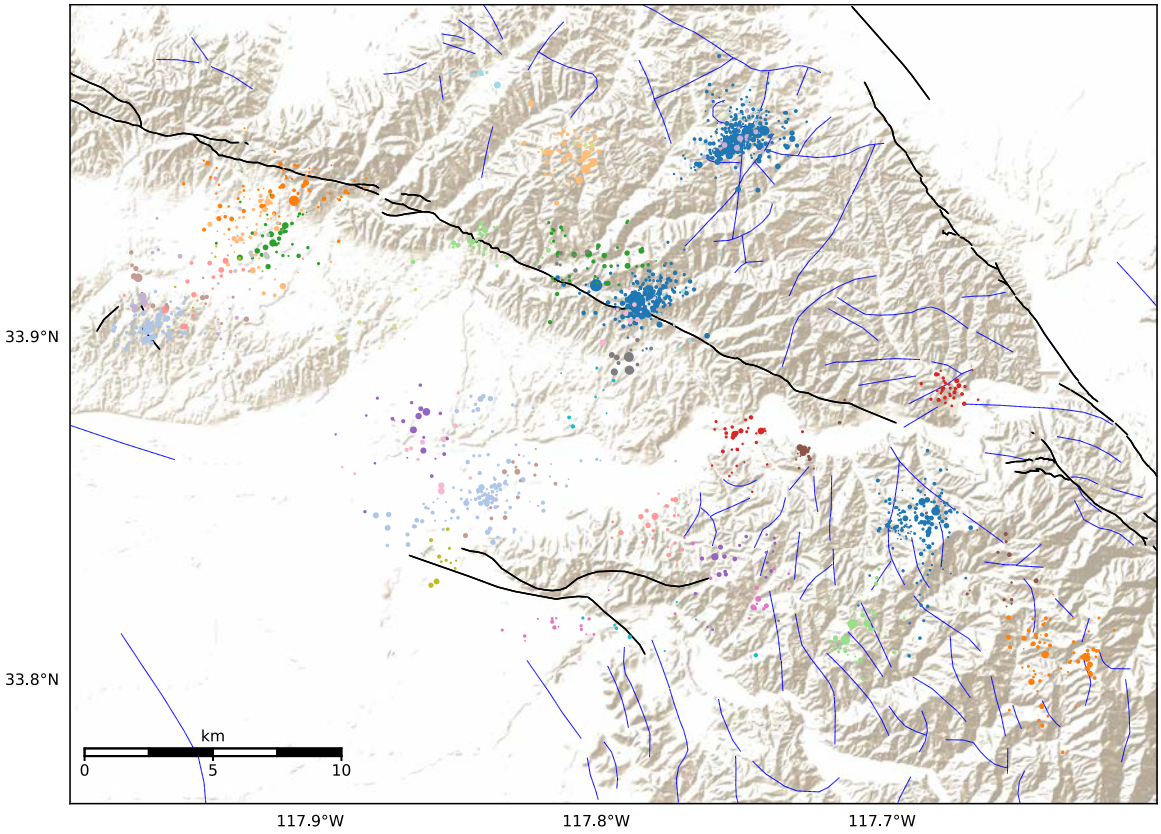

Figure 66: Map showing all major clusters of relocated events using the IASP91 velocity model with a 0.6 RMS differential travel time residual parameter. Only clusters that contained at least eight events are plotted. Events plotted as in Figure 27. Cluster numbers and centroids are indicated in Figure 66

The clusters making up the primary sequences within the research area bear similarities to those of the 0.2 RMS IASP91 velocity model relocations. The Yorba Linda Cluster retains its high angle orientation to the Whittier Fault. Interestingly, the large M 4.78 earthquake, which is a part of the primary cluster of this sequence, is at a considerable distance from the remainder of the cluster, deviating from the relatively close relocation of this event that is seen in the 0.2 RMS IASP91 velocity model relocations (Figure 66). For these relocation results, the Chino Hills Sequence is made up of three clusters (Figure 67). The overall shape of the sequence is less linear and more rounded, unlike the 0.2 RMS IASP91 velocity model relocation results, which showed a more elongated cluster.

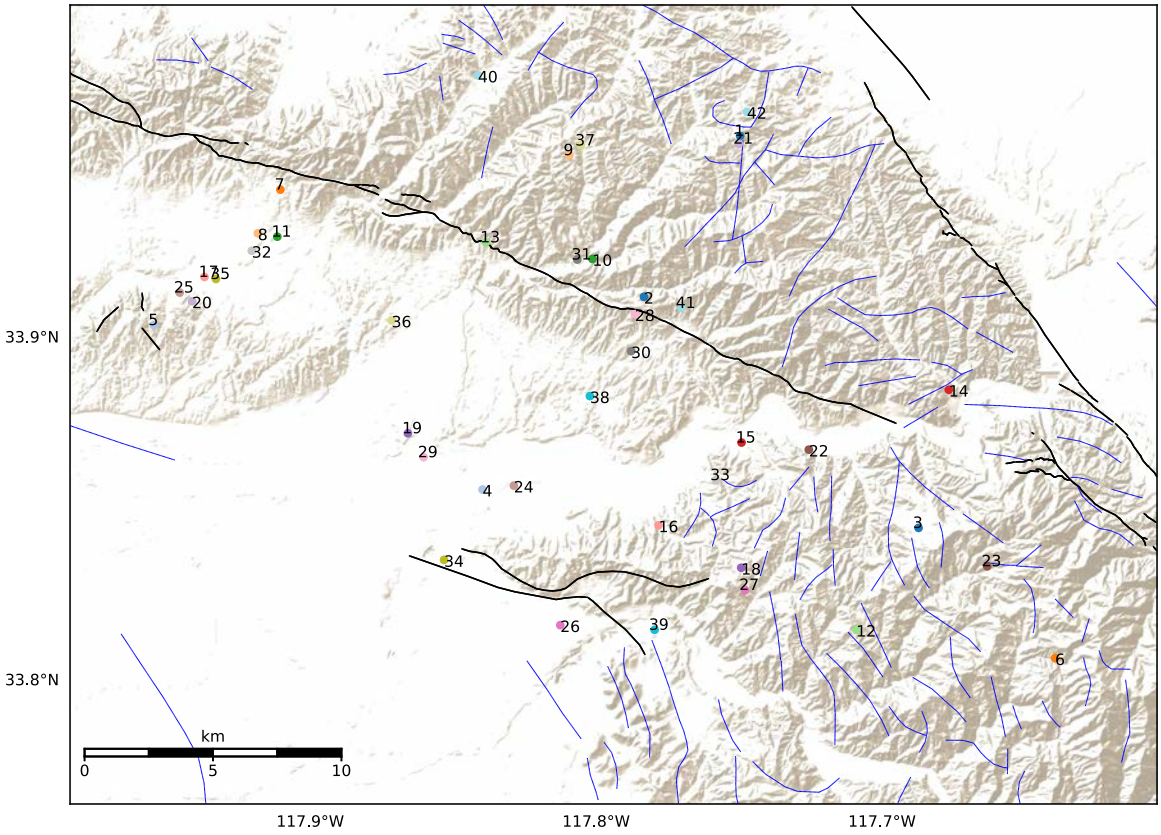

Figure 67: Map of the clusters of the IASP91 velocity model relocation results with a 0.6 RMS differential travel time residual parameter. Labels and circles as in Figure 28.

The RMS residual P-wave differential times for these relocation results bear similarities to the other relocation results (Figure 68). However, the number of events that have a residual between 0.25 and 0.3 seconds is remarkably high while these results have a higher average and wider spread than those of the 0.2 RMS IASP91 velocity model relocation results. Figures 69 and 70 have events plotted color coded by their respective RMS residual P- and S-wave differential times.

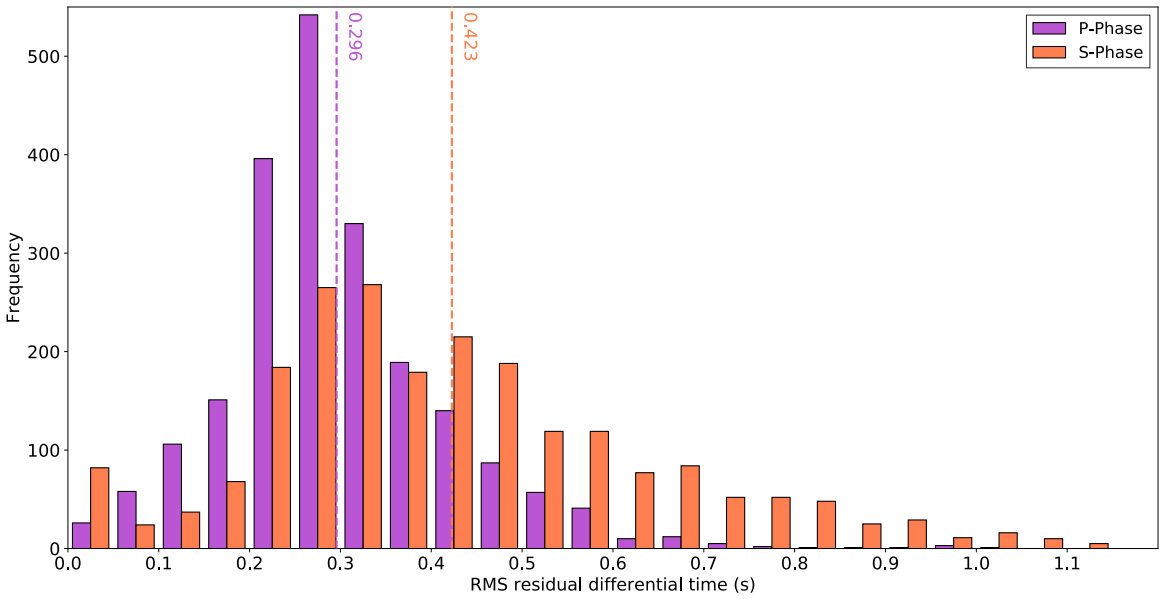

Figure 68: Histogram showing the RMS residual differential times for the P-wave and S-wave for relocated events using the IASP91 velocity model under the 0.6 RMS differential travel time residual parameter. Lines as shown in Figure 29.

As seen with the 0.2 RMS relocation results, the Yorba Linda and Chino Hills Sequences have distinctly low differential times. Like all other relocation results, for the La Habra Sequence the majority of events possess medium to high RMS residual P-wave differential times as well as much higher RMS residual S-wave differential times. (Figure 69, Figure 70). Clusters toward the southwest of the Yorba Linda Sequence make up the other tightly constrained collection just southwest from the Yorba Linda Sequence and contain higher RMS residual P-wave and S-wave differential times (Figure 69, Figure 70).

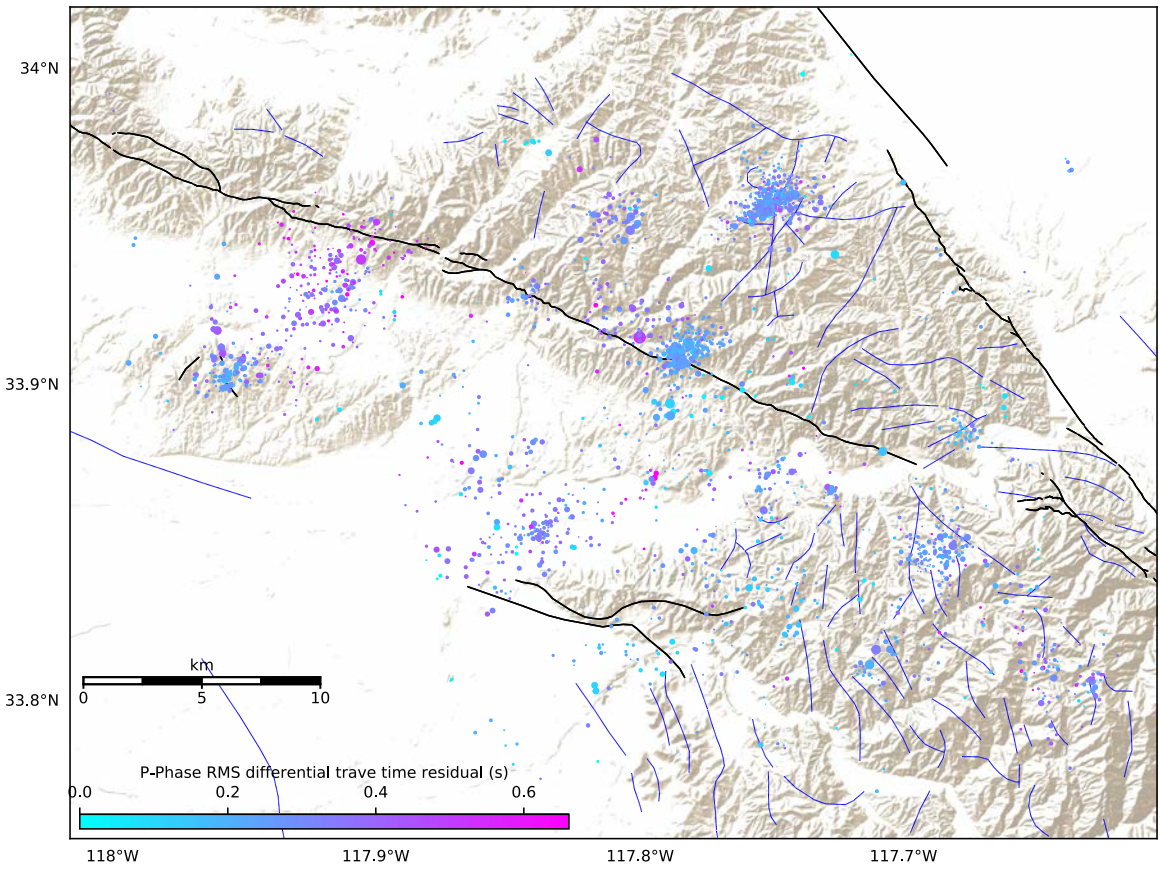

Figure 69: Map of relocated events color coded by their respective RMS residual P-wave differential time from the IASP91 velocity model relocation results under a 0.6 RMS differential travel time residual parameter.

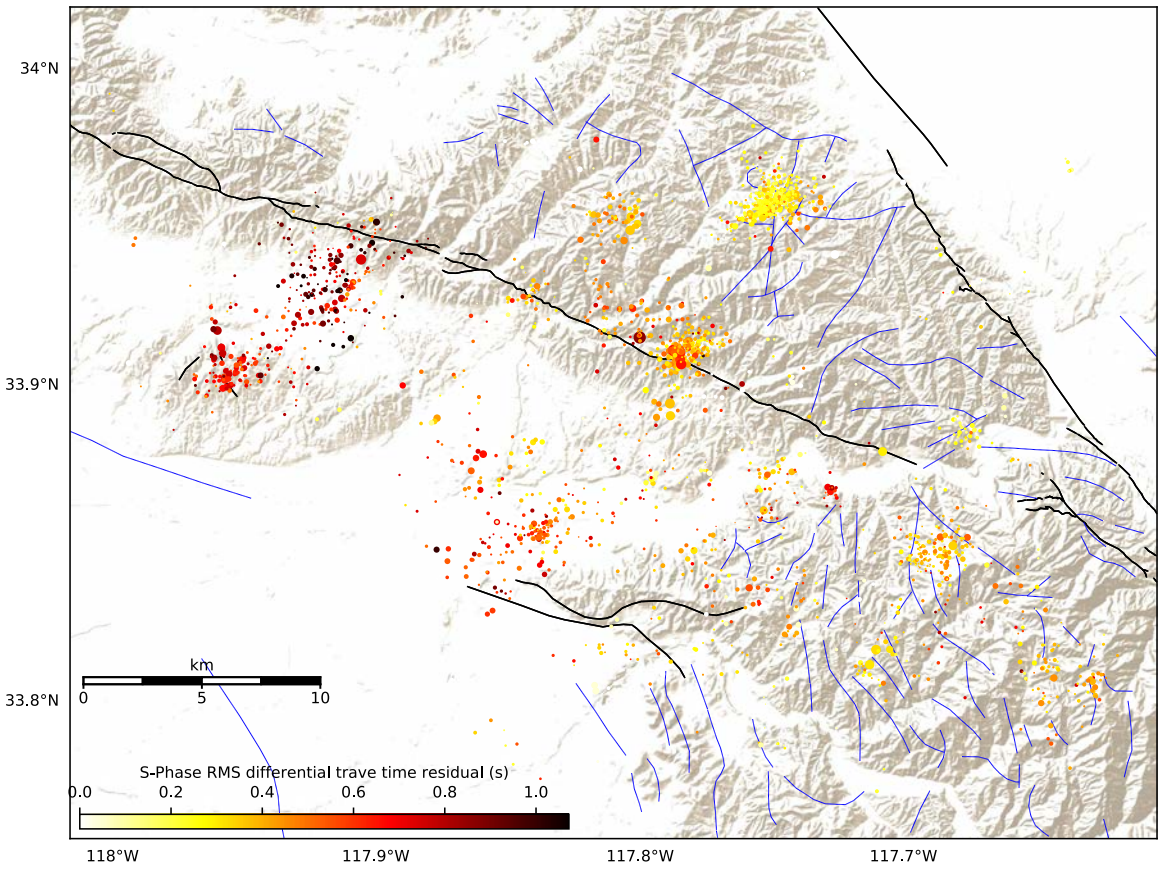

Figure 70: Map of relocated events color coded by their respective RMS residual S-wave differential time from the IASP91 velocity model relocation results under a 0.6 RMS differential travel time residual parameter.

The location errors of the IASP91 velocity model relocation results are shown in Figure 71. The horizontal location errors for the 0.6 RMS IASP91 velocity model relocations have a smaller average error, despite having a larger distribution than the horizontal errors of the 0.2 RMS relocation results for the same velocity model. Interestingly, the vertical errors for both RMS results of the IASP91 velocity model have the same average, but the 0.6 RMS relocations have a significantly larger distribution. The horizontal and vertical errors of each event were also plotted in Figures 72 and 73.

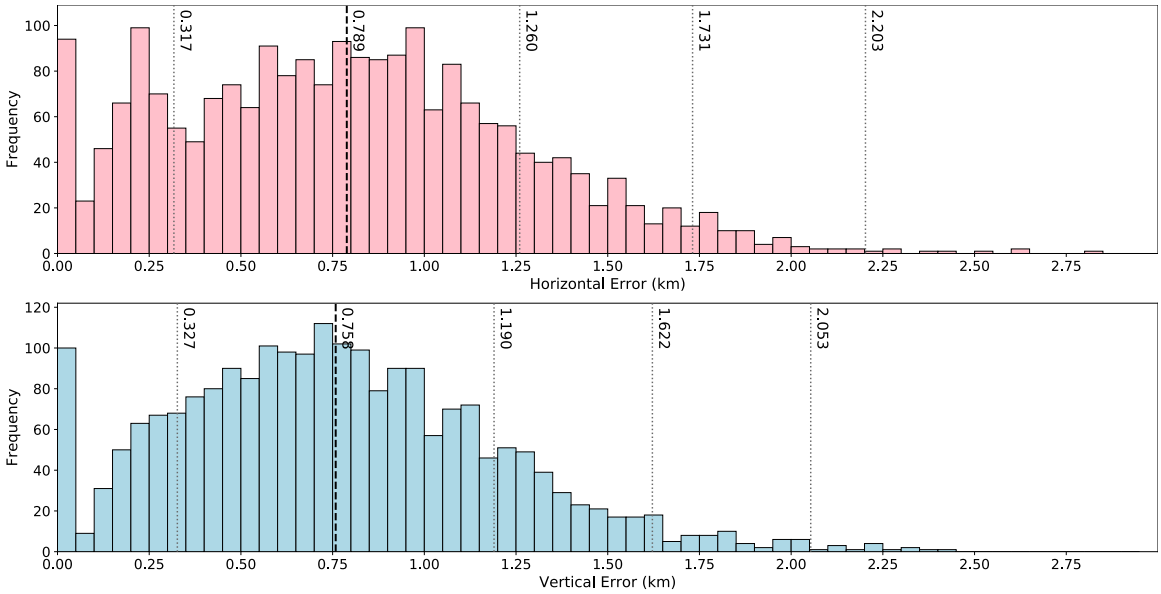

Figure 71: Histograms showing the horizontal and vertical location errors for IASP91 velocity model relocation results under a 0.6 RMS differential travel time residual parameter.

We can see that higher RMS residual P- and S-wave differential times are associated with considerable location errors. Like their 0.2 RMS counterparts, the Yorba Linda and Chino Hills Sequences possess small vertical and horizontal errors, aside from the few larger location errors associated with the smaller clusters within both of the sequences (Figure 72, Figure 73). As expected, the La Habra Sequence possesses events with higher than average location errors. The clusters making up the assemblage of events southwest from the Yorba Linda Sequence (Clusters 4, 19, 24, 29, and 34) are also made up of events with relatively large location errors (Figure 72, Figure 73).

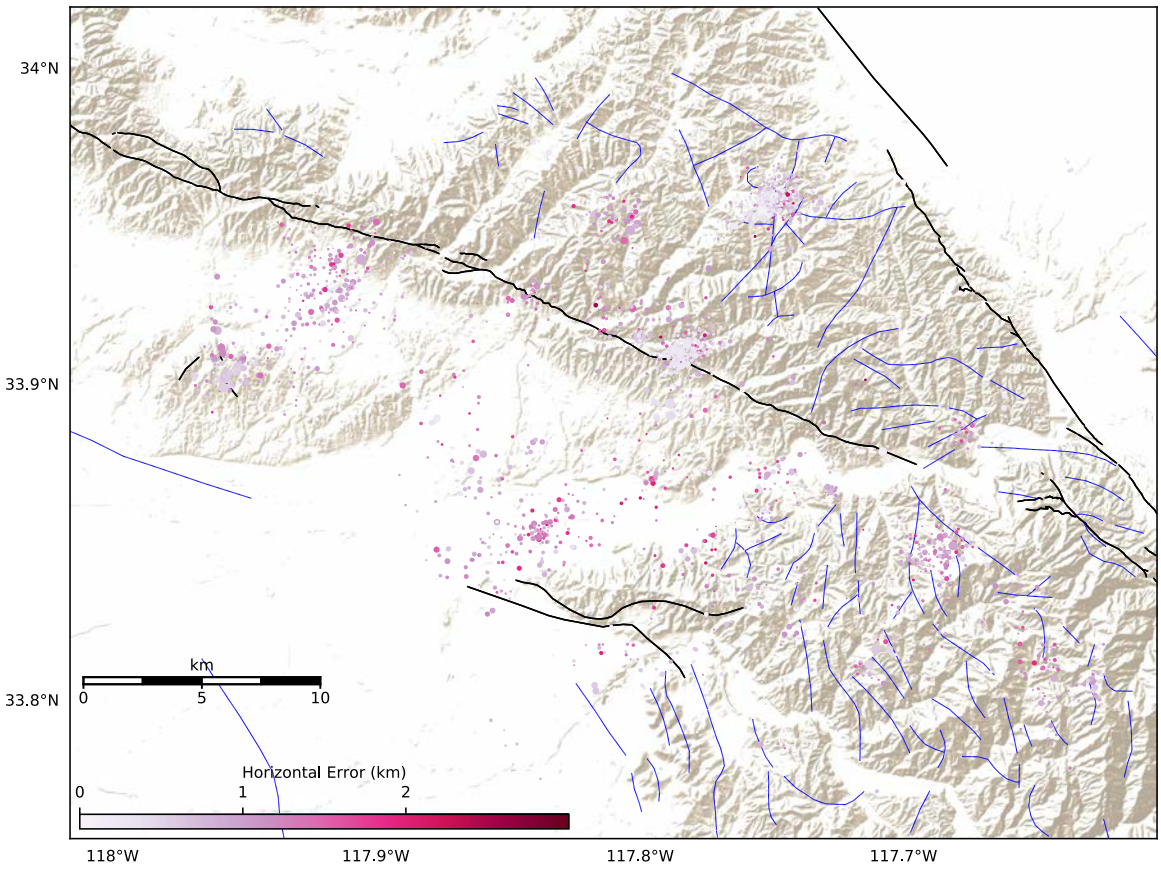

Figure 72: Map of the horizontal errors for of each relocated event using the IASP91 velocity model with a 0.6 RMS differential travel time residual parameter.

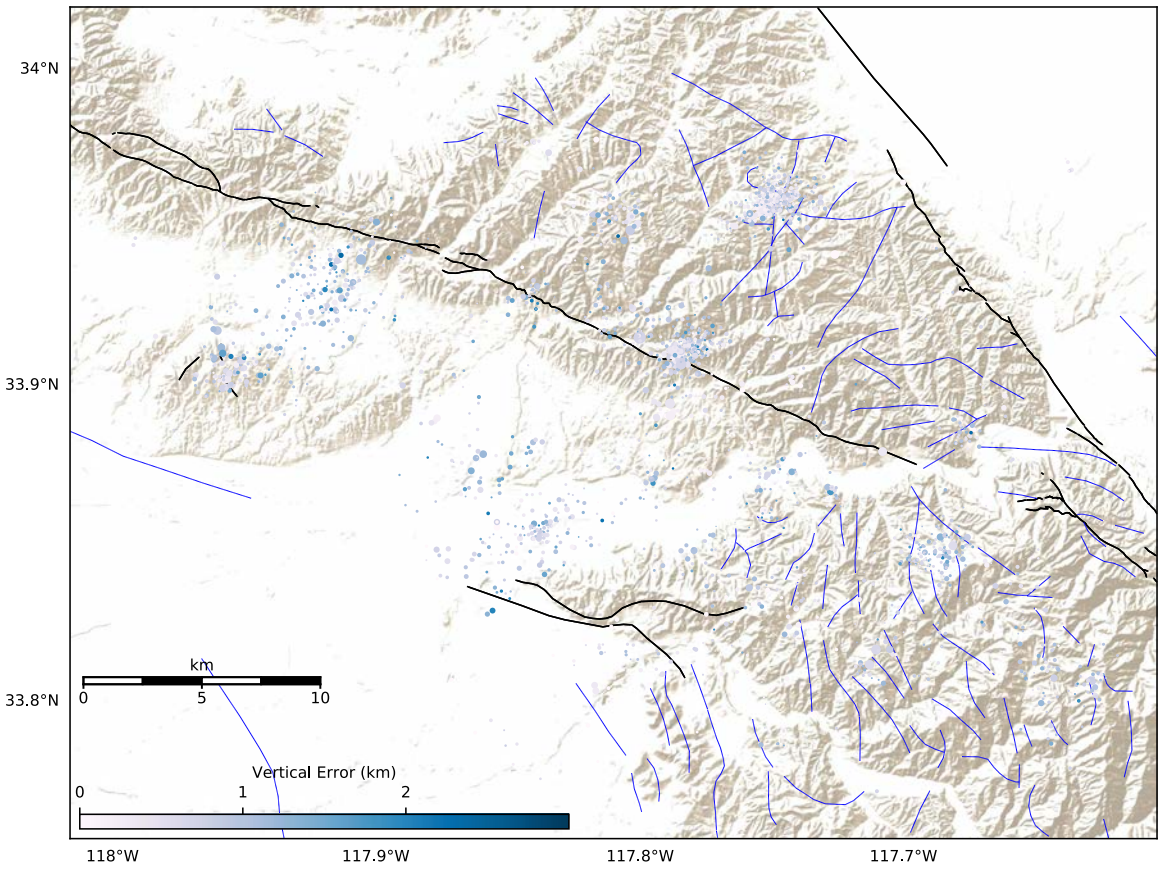

Figure 73: Map of the vertical errors associated with the relocation of events using the IASP91 velocity model with a 0.6 RMS differential travel time residual.

3.2.2 Smoothed Southern California Velocity Model Relocation Results

The GrowClust algorithm using a 0.6 RMS differential travel time residual parameter and the smoothed southern California velocity model successfully relocated 2186 of the 4434 events, more than the 2143 relocated events for the 0.2 RMS relocation results for the same velocity model (Table 3). These relocation results show a similar number of events relocated as the previous relocation results. The distribution of relocated distances shows a large number of events relocated at smaller distances than for prior results (Figure 74). Original and relocated locations of every event relocated using this velocity model and RMS differential travel time residual can be viewed in Appendix C: Figure 110 and Appendix D: Figure 113, respectively.

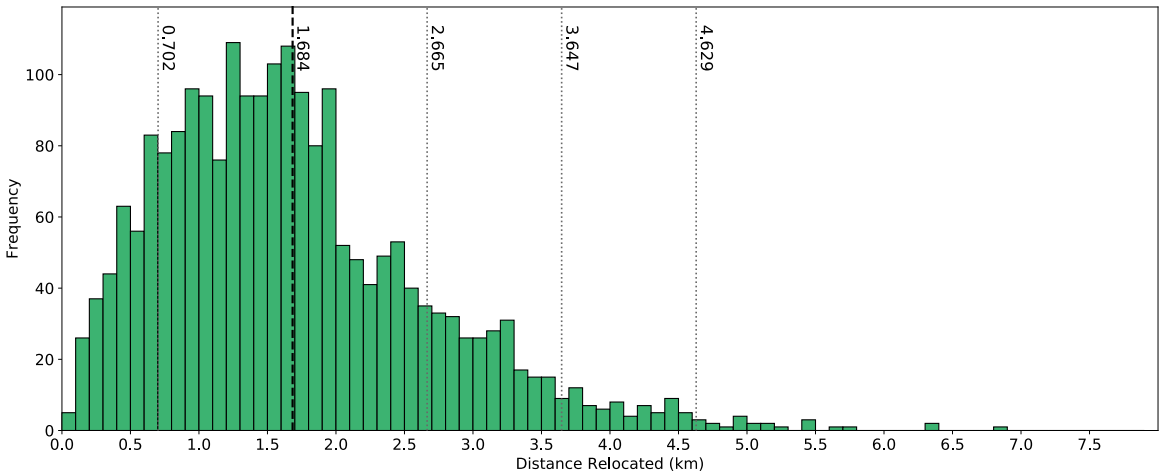

Figure 74: Histogram showing the frequency of events relocated to their new locations using the smoothed southern California velocity model under a 0.6 RMS differential travel time residual parameter as a function of distance between the original and relocated event location. Labels and lines as in Figure 45.

The Yorba Linda Sequence possesses events that have been relocated at relatively small distances, particularly those within the largest cluster of the Sequence (Figure 75). Unlike the 0.2 RMS smoothed southern California velocity model relocations, these results show a single assemblage of earthquakes as opposed to two separate groupings (Figure 75). The M 4.78 event has been relocated to a different location than its 0.2 RMS counterpart and possesses a larger than average relocation distance value. The Chino Hills Sequence has more events that were relocated at larger distance than previously seen in the 0.2 RMS smoothed southern California velocity model relocation results. The La Habra Sequence continues the trend of having a wide variety of different relocated distances.

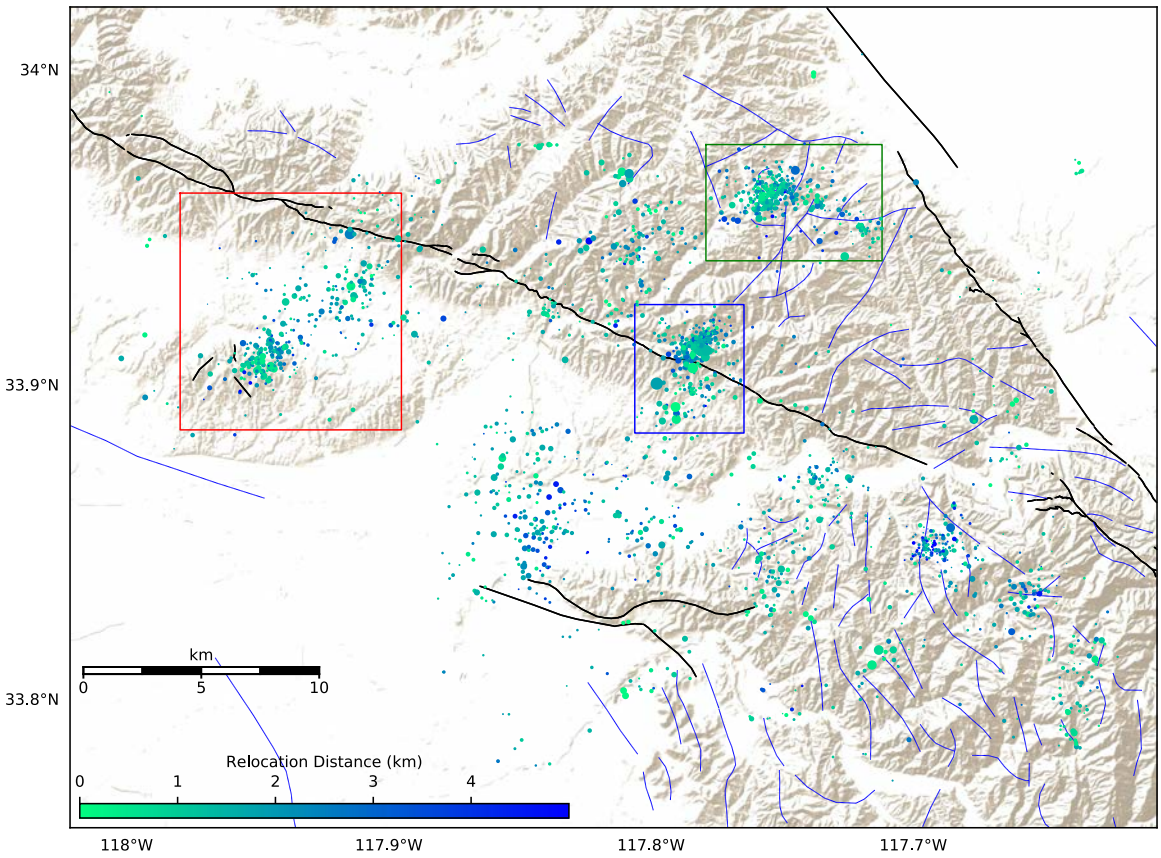

Figure 75: Map of relocated events color coded by the distance each event was relocated compared to its original location, using the smoothed southern California velocity model with a 0.6 RMS differential travel time residual. The blue box outlines the Yorba Linda Sequence (Figure 94-ii), the green box denotes the location of the Chino Hills Sequence (Figure 97-ii), and the red box represents the La Habra Sequence (Figure 100-ii).

The 2186 relocated events in these relocation results were compiled into 298 clusters, more than that of the IASP91 relocation results. Of these 298 cluster, 46 of them are assemblages of eight or more events. This is a decrease compared to the 53 clusters from the 0.2 RMS relocations for the smoothed southern California velocity model. The clusters are displayed in Figure 76 while the number identification and cluster centroid of these clusters are shown in Figure 77. There are significant differences in the cluster densities of these relocation results compared to the prior relocation results. The Chino Hills Sequence, in particular, has become less consolidated and less linear in shape compared to the 0.2 RMS smoothed southern California velocity model relocations. The second largest cluster in the sequence has a curvature to it while intersecting the main cluster along the southeast

edge (Figure 76). The Yorba Linda Sequence also displays a considerable difference in the shape of the trend compared to the IASP91 relocation results.

The La Habra Sequence, as the other two primary sequences, shows a considerable difference in the location of the clusters that make up this sequence (Figure 76). The La Habra Sequence retains its two assemblages of clusters as seen for other previous relocation results (Figure 76). The clusters situated further southeast from the Yorba Linda Sequence (Clusters 5, 14, 25, 31, 32, 33, and 34) have become more dispersed than those of 0.2 RMS counterpart relocation results (Figure 76). The remainder of the clusters in the southeast region have also become less consolidated. While there are fewer clusters in the southeast corner of the research area, compared to the 0.2 RMS relocations, they are more tightly constrained.

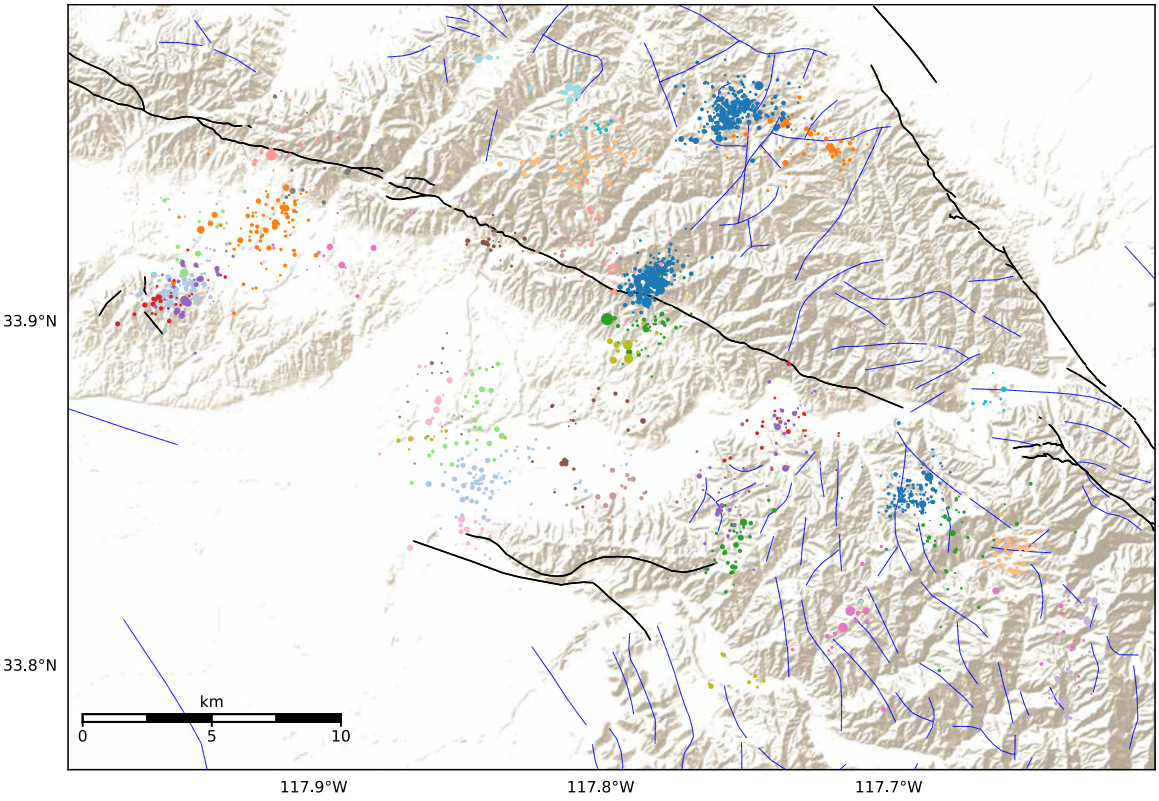

Figure 76: Map showing all major clusters of relocated events using the smoothed southern California velocity model with a 0.6 RMS differential travel time residual parameter. Events plotted as in Figure 27. Cluster numbers and centroids are indicated in Figure 76

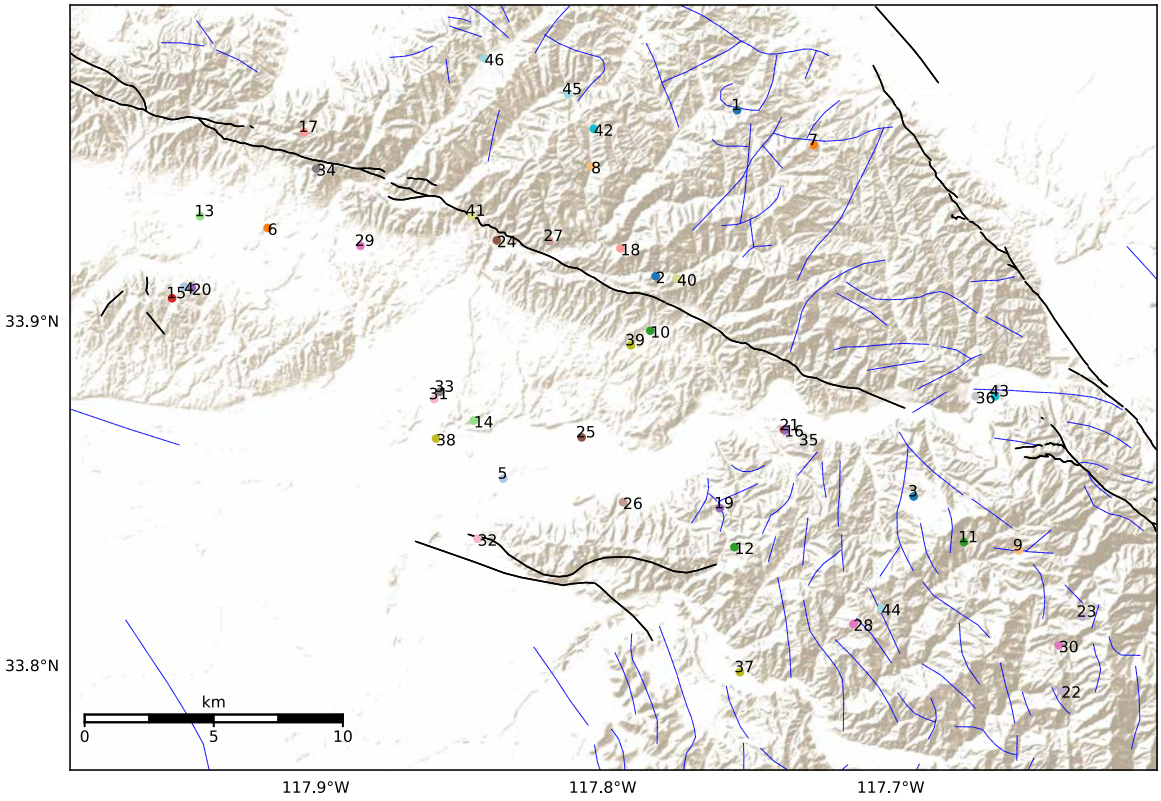

Figure 77: Map of the clusters of the smoothed southern California velocity model relocation results with a 0.6 RMS differential travel time residual parameter. Labels and circles as in Figure 28.

The differential times of the relocation results using the smoothed southern California velocity model presents a similar distribution as those of 0.2 RMS smoothed southern California velocity model relocations (Figure 78). Figures 79 and 80 have plotted events with their respective differential times.

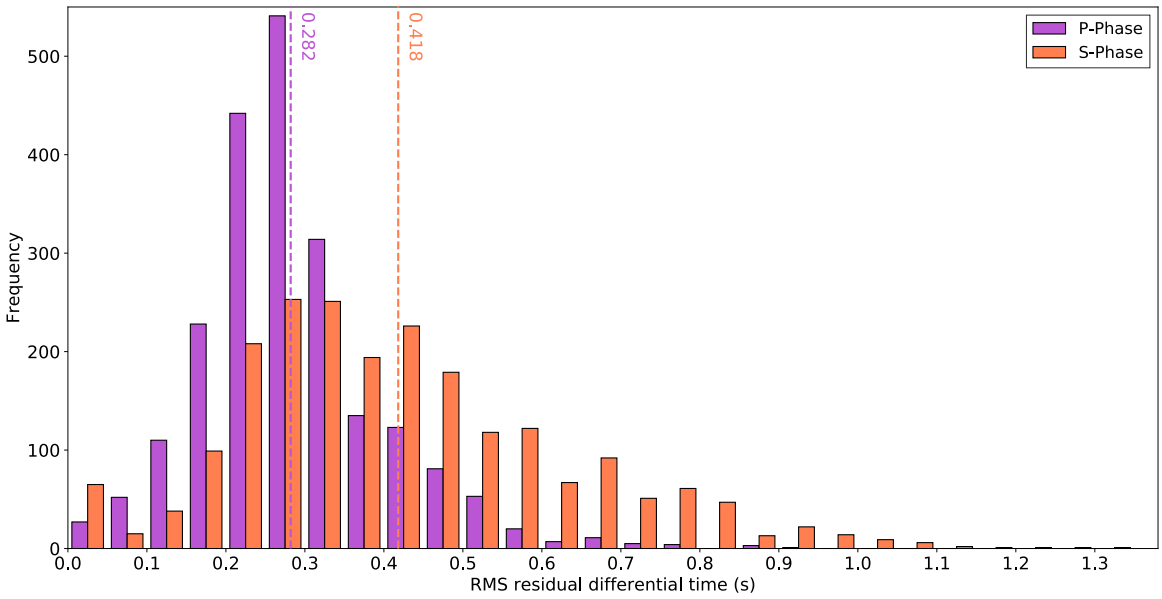

Figure 78: Histogram showing the RMS residual differential times for the P-wave and S-wave for relocated events using the smoothed southern California velocity model under the 0.6 RMS differential travel time residual parameter. The purple dashed line denotes the average RMS P-wave residual differential time while the orange dashed line denotes the average RMS S-wave residual differential time.

As mentioned previously, the Yorba Linda Sequence possesses smaller RMS residual P-wave differential times than those seen in the 0.2 RMS relocations for the same velocity model. The S-wave differential times are similar throughout the sequence, while the larger magnitude events have higher differential times (Figure 80). As for the 0.2 RMS relocation results for the smoothed southern California velocity model, the Chino Hills Sequence is made up of low RMS residual P-wave differential times for these relocation results (Figure 79). As with the 0.2 RMS relocation results for the same velocity model, the La Habra Sequence bears high RMS residual S-wave arrival times (Figure 80).

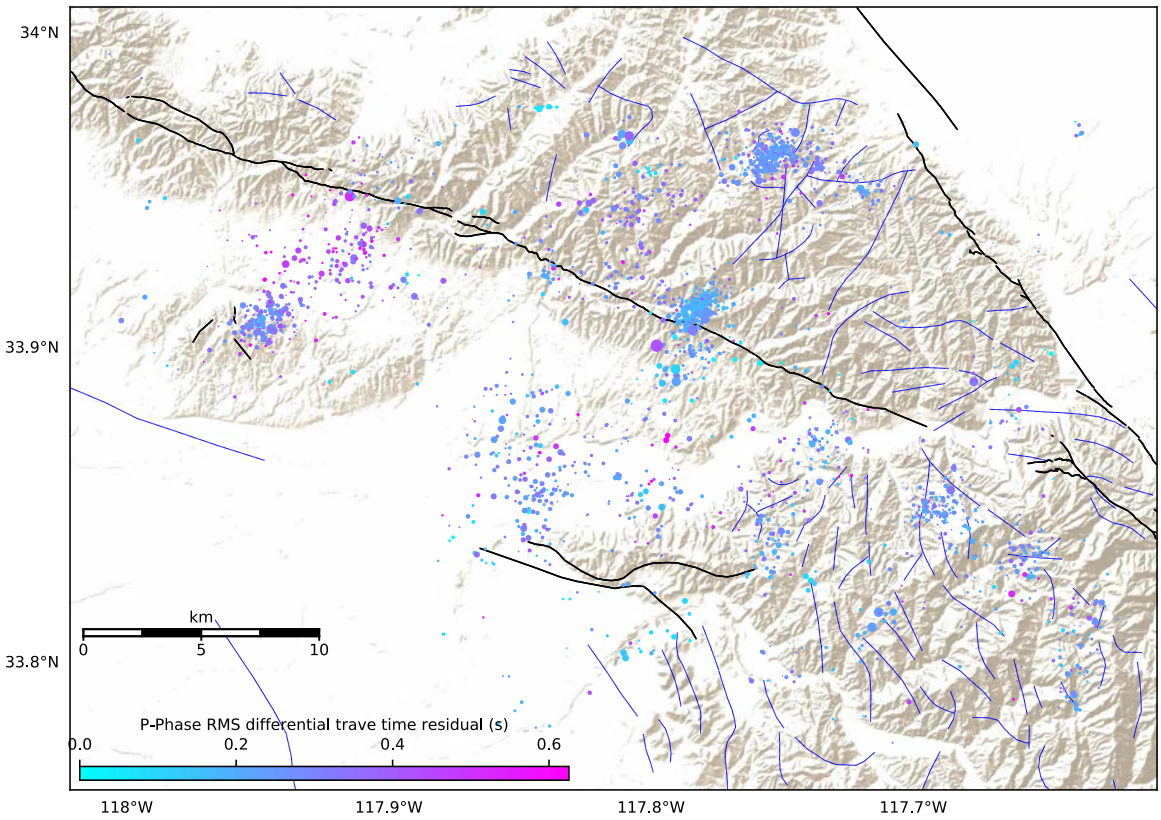

Figure 79: Map of relocated events color coded by their respective RMS residual P-wave differential time from the smoothed southern California velocity model relocation results under a 0.6 RMS differential travel time residual parameter.

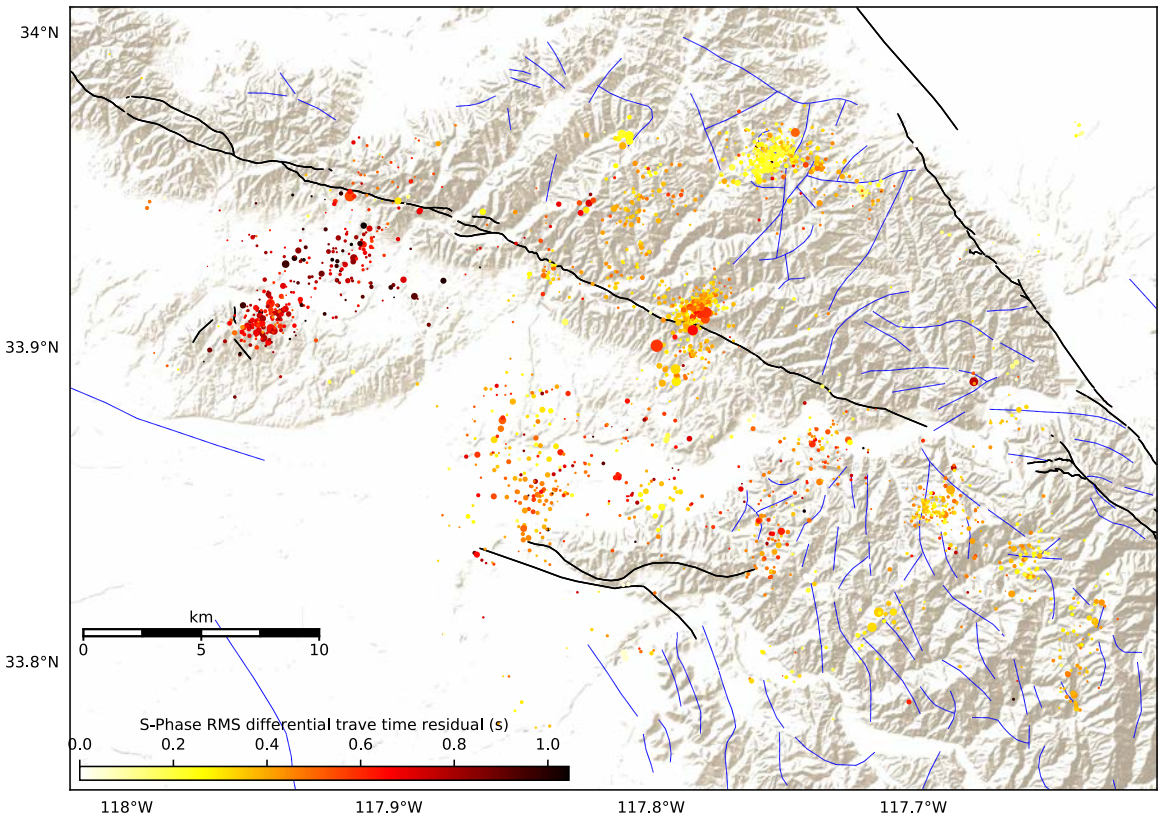

Figure 80: Map of relocated events color coded by their respective RMS residual S-wave differential time from the smoothed southern California velocity model relocation results under a 0.6 RMS differential travel time residual parameter.

In tandem with the differential times, the location errors of the 0.6 RMS smoothed southern California velocity model relocation results also appear to be lower than for the previous model (Figure 81. The average horizontal error for these relocation results is very similar to the 0.2 RMS relocations for the same velocity model, whereas the average vertical location error is lower than the same other smoothed southern California velocity model relocations. The distribution of the errors for these results has a wider spread for the horizontal errors than 0.2 RMS counterpart relocations (Figure 81). Conversely, the distribution is smaller for the vertical errors. These errors are plotted for every relocated event in Figures 82 and 83.

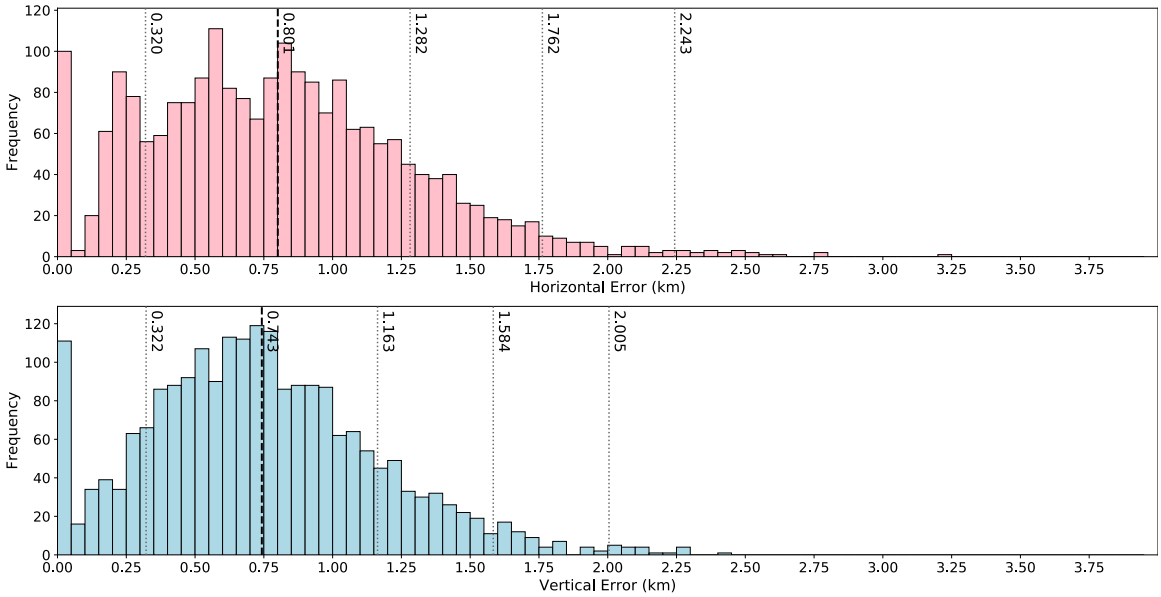

Figure 81: Histograms showing the horizontal and vertical location errors for smoothed southern California velocity model relocation results under a 0.6 RMS differential travel time residual parameter.

Overall, the location errors of each of the clusters bear strong similarity to those of the 0.2 RMS smoothed southern California relocations. Both the Yorba Linda and Chino Hills Sequences have very low horizontal errors while the La Habra Sequence has high horizontal errors (Figure 82). The same observations can be made for the vertical errors (Figure 83). There are distinctly lower horizontal errors across the majority of the events in both the Yorba Linda and the Chino Hills Sequences. While the La Habra Sequence does have higher location errors than the other two main sequences, these relocation results do have lower errors than the IASP91 velocity model relocation results.

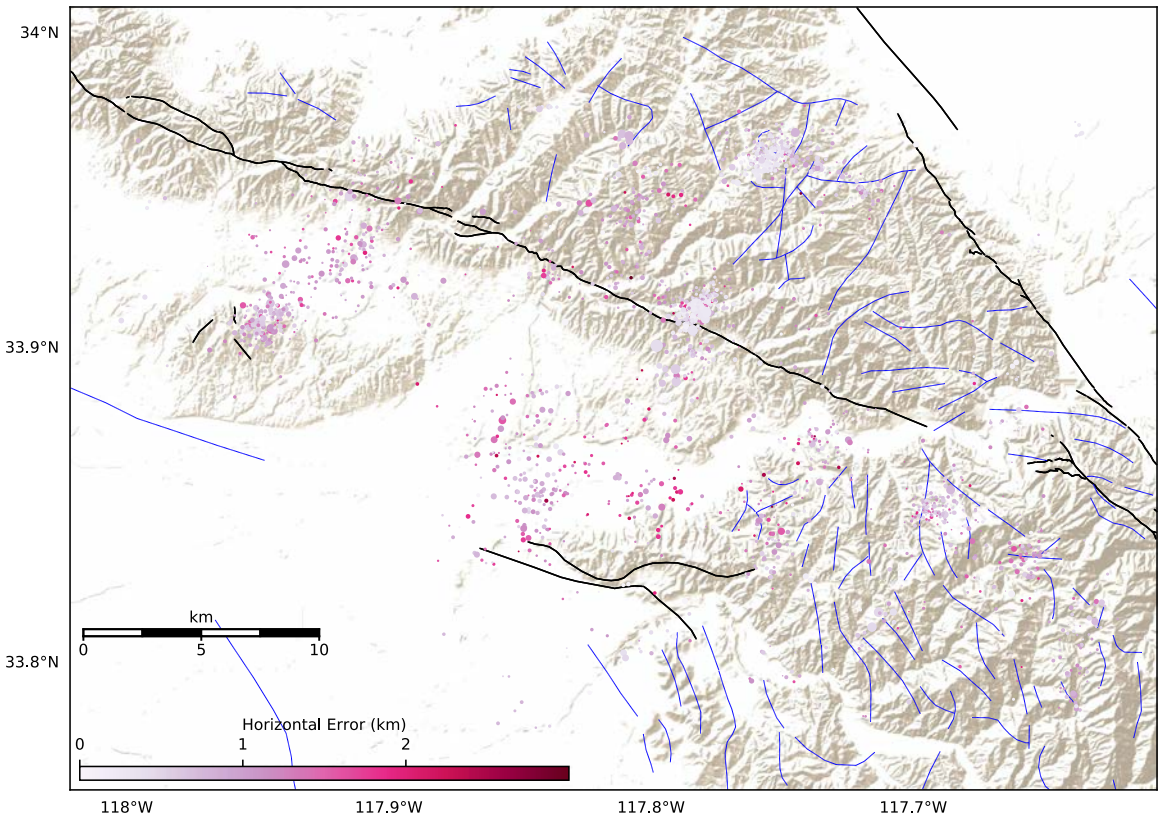

Figure 82: Map of the horizontal errors for of each relocated event using the smoothed southern California velocity model with a 0.6 RMS differential travel time residual parameter.

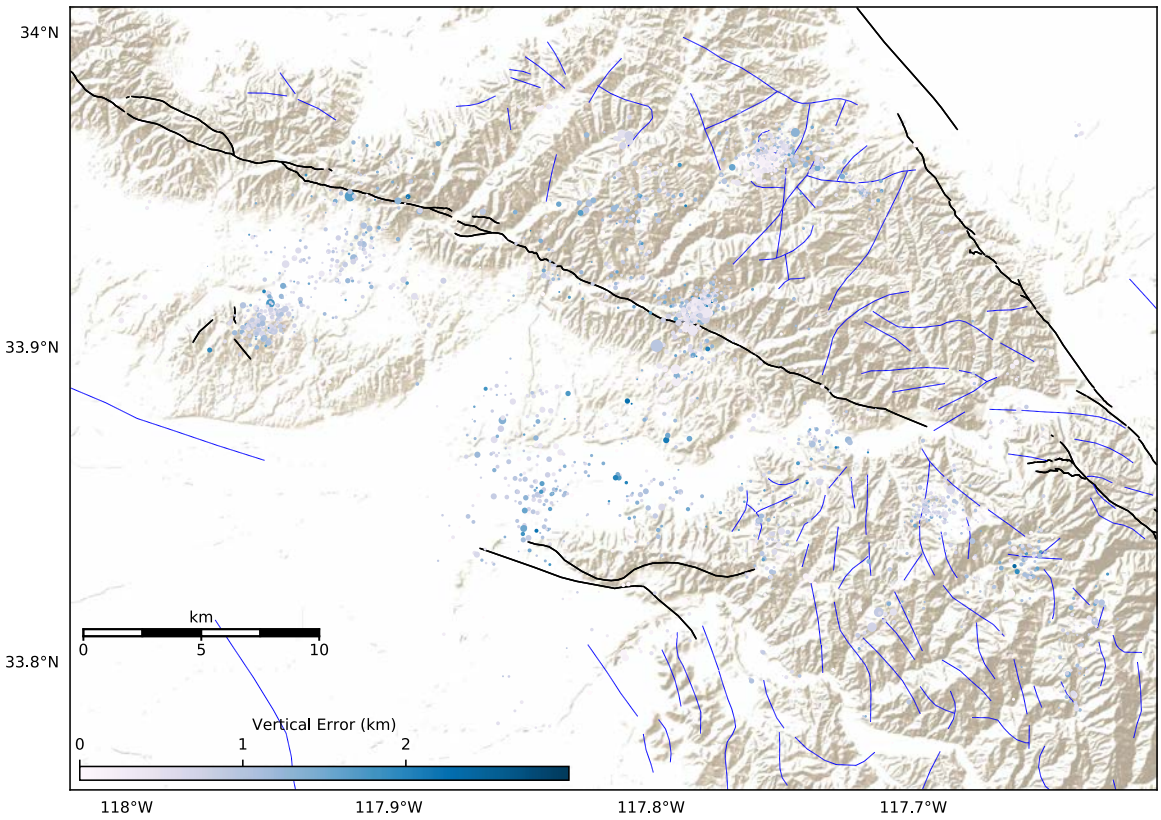

Figure 83: Map of the vertical errors associated with the relocation of events using the smoothed southern California velocity model with a 0.6 RMS differential travel time residual.

3.2.3 Los Angeles Basin Velocity Model Relocation Results

Of the 4434 catalog events that were entered into the GrowClust algorithm, 2225 events were successfully relocated under a 0.6 RMS differential travel time residual parameter and the utilization of the LA Basin velocity model (Table 3). These relocation results have the largest number of successful relocations of any model. Figure 84 shows a histogram of relocated distances of these results. Events with their respective relocated distance are then plotted in Figure 85. Original locations and relocated locations of every event relocated with respect to depth using this velocity model and RMS differential travel time residual can be viewed in Appendix C: Figure 111 and Appendix D: Figure 114, respectively.

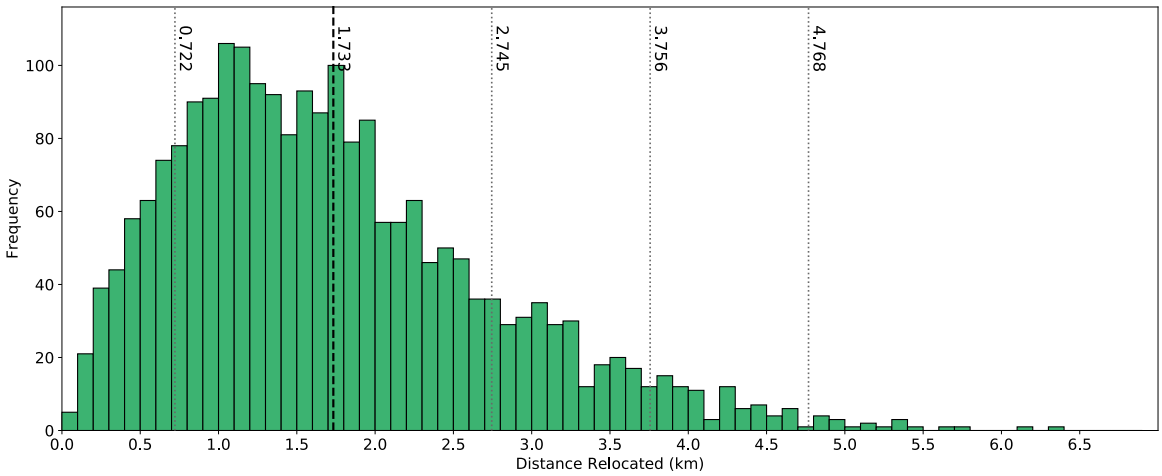

Figure 84: Histogram showing the frequency of events relocated to their new locations using the LA Basin velocity model under a 0.6 RMS differential travel time residual parameter as a function of distance between the original and relocated event location. The black dashed line denotes the average distance relocated, while the dotted gray lines represent the standard deviations, up to 3σ.

A large majority of the events that were adjusted at larger distances from their original location are located outside of the the Yorba Linda and Chino Hills Sequences, as was seen with the 0.2 RMS LA Basin velocity model relocations (Figure 85). Aside from the main sequence, other events that possess large relocation distance are located just southwest of the Yorba Linda Sequence and towards the southwest as well as the clusters located in the southeastern portion of the map (Figure 85).

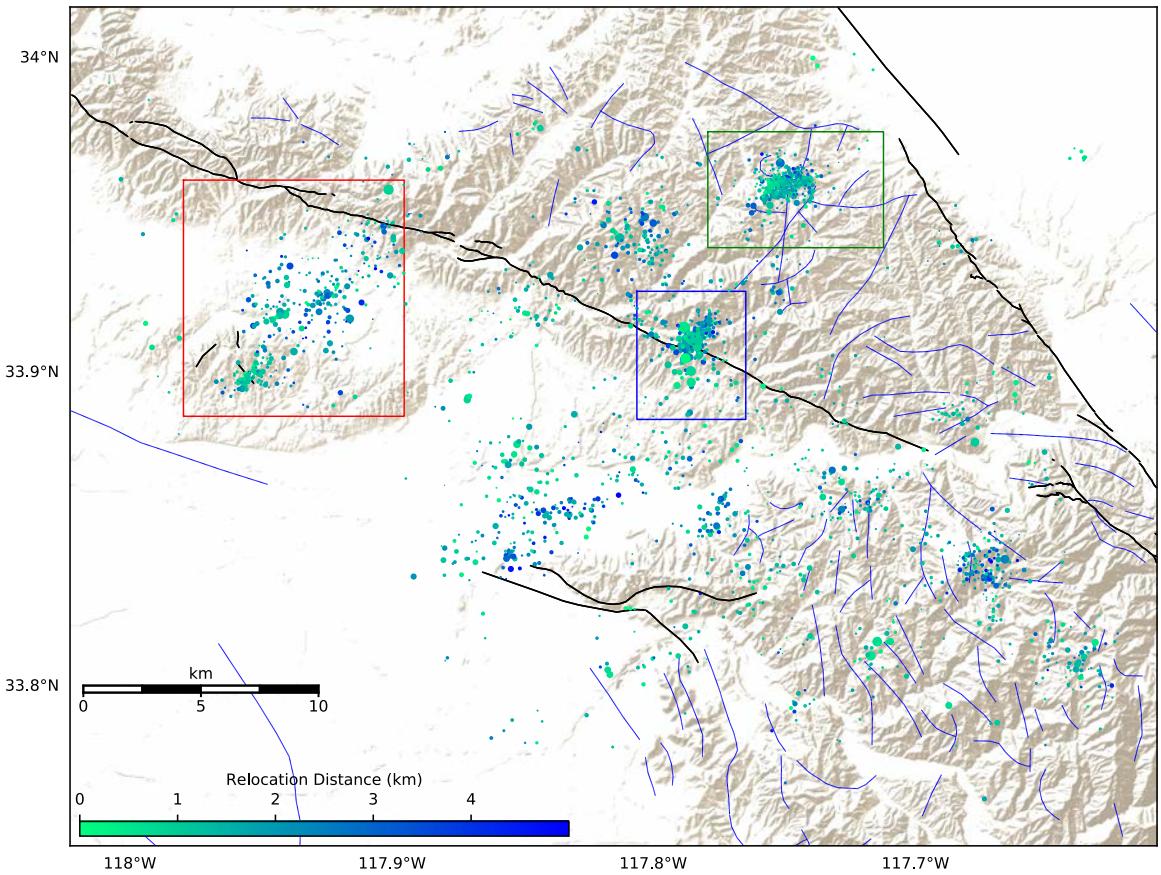

Figure 85: Map of relocated events color coded by the distance each event was relocated compared to its original location, using the LA Basin velocity model with a 0.6 RMS differential travel time residual. The blue box outlines the Yorba Linda Sequence (Figure 94-iii), the green box denotes the location of the Chino Hills Sequence (Figure 97-iii), and the red box represents the La Habra Sequence (Figure 100-iii).

The GrowClust algorithm consolidated the 2225 relocated events into 298 events. Of all relocation results, these results present the fewest clusters and the highest number of relocated events. Only 45 of these clusters have a collection of at least eight events within them, less than the 52 clusters formed for the 0.2 RMS relocations for the same velocity model. These clusters are plotted in Figure 86 while the respective cluster centroids and identification number are shown in Figure 87. The majority of the clusters are more condensed than for the two previous 0.6 RMS models, as well as the 0.2 RMS LA Basin velocity model relocations (Figure 86). Three of the clusters towards the southeast from the Yorba Linda Sequence (Clusters 5, 18, 25, and 35) have formed into the elongated linear shape that is also seen in the 0.2 RMS LA Basin velocity model relocation results

(Figure 86, Figure 87).

The Chino Hills Sequence is composed of only two clusters and has become more elliptical in shape as opposed to the thin elongated trend observed in the 0.2 RMS results for the same velocity model (Figure 86). The Yorba Linda Sequence, made up of two clusters (Clusters 2 and 14), has become more consolidated than what was seen in the 0.2 RMS LA Basin velocity model relocation results (Figure 86). The La Habra Sequence, consisting of five clusters, has become more consolidated in shape (Figure 86). The events within this sequence are spread throughout the entirety of the trend, filling in the gaps that were seen in prior relocation results. An interesting observation between these relocation results and the 0.2 RMS relocation results of the same velocity model is that the 2014 La Habra mainshock is no longer successfully relocated.

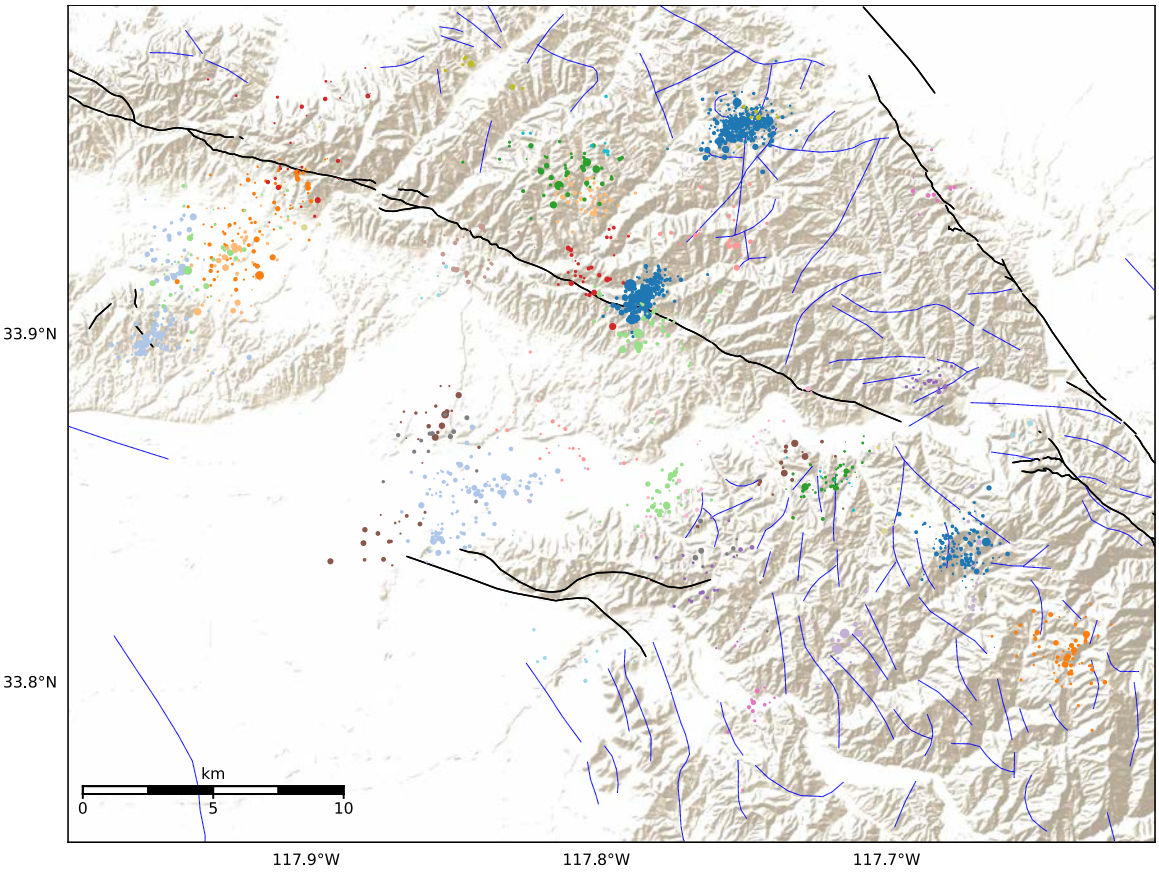

Figure 86: Map showing all major clusters of relocated events using the LA Basin velocity model with a 0.6 RMS differential travel time residual parameter. Only clusters that contained at least eight events are plotted. Events plotted as in Figure 27. Cluster numbers and centroids are indicated in Figure 86

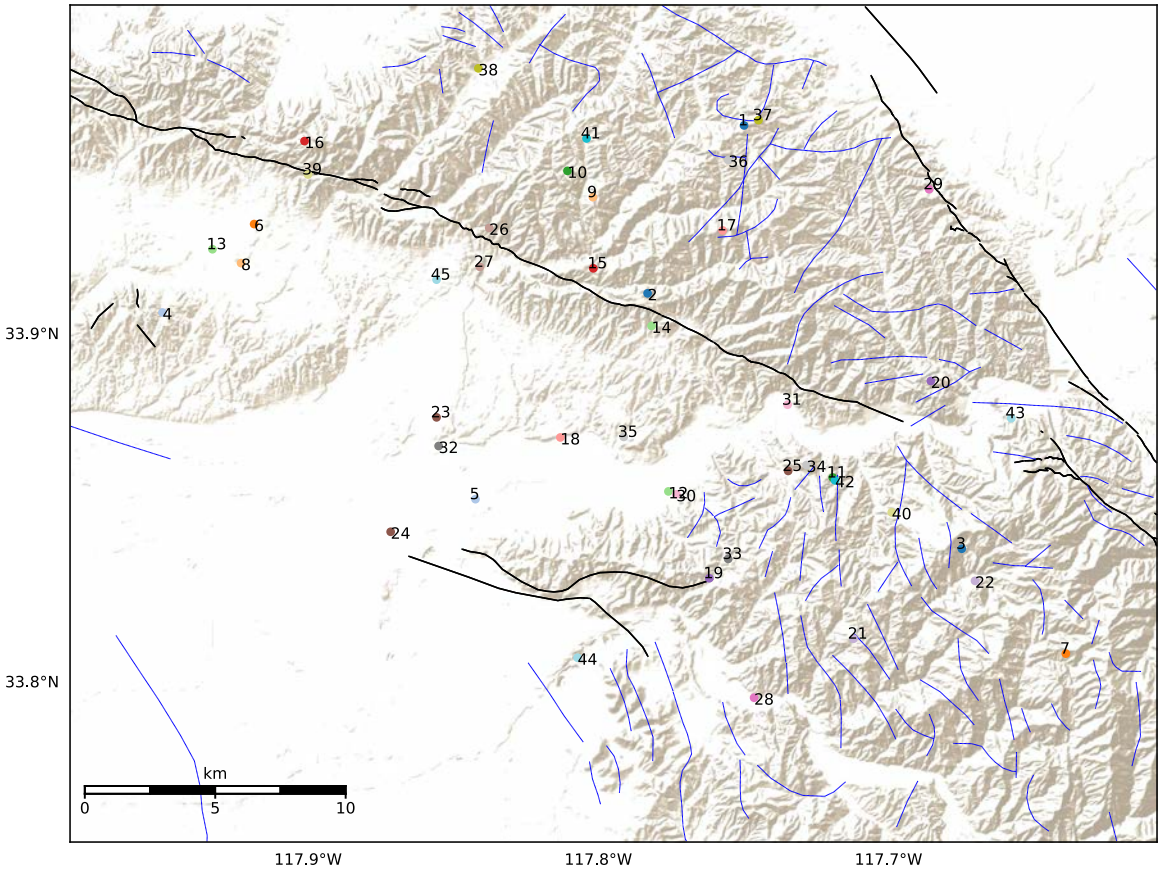

Figure 87: Map of the clusters of the LA Basin velocity model relocation results with a 0.6 RMS differential travel time residual parameter. Labels and circles as in Figure 28.

Figure 88 shows the distribution of RMS differential times for these relocation results. As expected, the majority of the relocated events have a differential RMS residual P-wave differential time between 0.2 and 0.3 s, similar to all of the other relocation results. Events with their RMS residual P- and RMS residual S-wave differential times are plotted on a map in Figures 89 and 90.

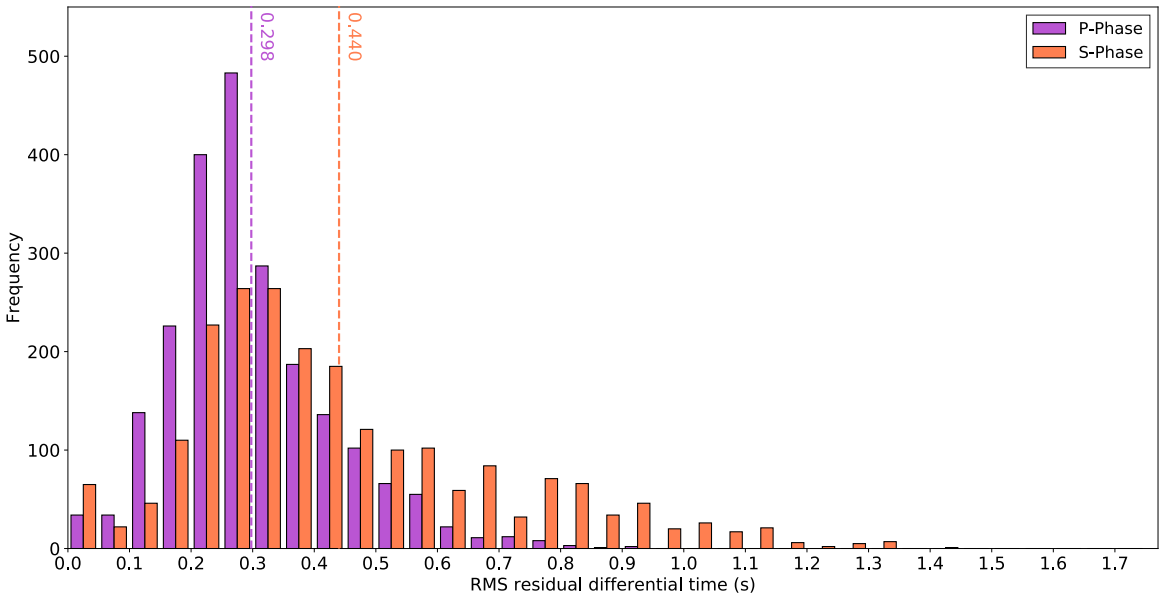

Figure 88: Histogram showing the RMS residual differential times for the P-wave and S-wave for relocated events using the LA Basin velocity model under the 0.6 RMS differential travel time residual parameter. The purple dashed line denotes the average RMS P-wave residual differential time while the orange dashed line denotes the average RMS S-wave residual differential time.

Similarly to other relocation results, the majority of the large RMS residual P-wave differential times are from the relocated events contained within the La Habra Sequence (Figure 66). Most of these high RMS residual P-wave differential times within the La Habra Sequence are at the northernmost end as well as along the northwest border of the sequence. Both the Yorba Linda and Chino Hills Sequences maintain their low RMS residual P-wave differential times from their 0.2 RMS relocation counterparts (Figure 89).

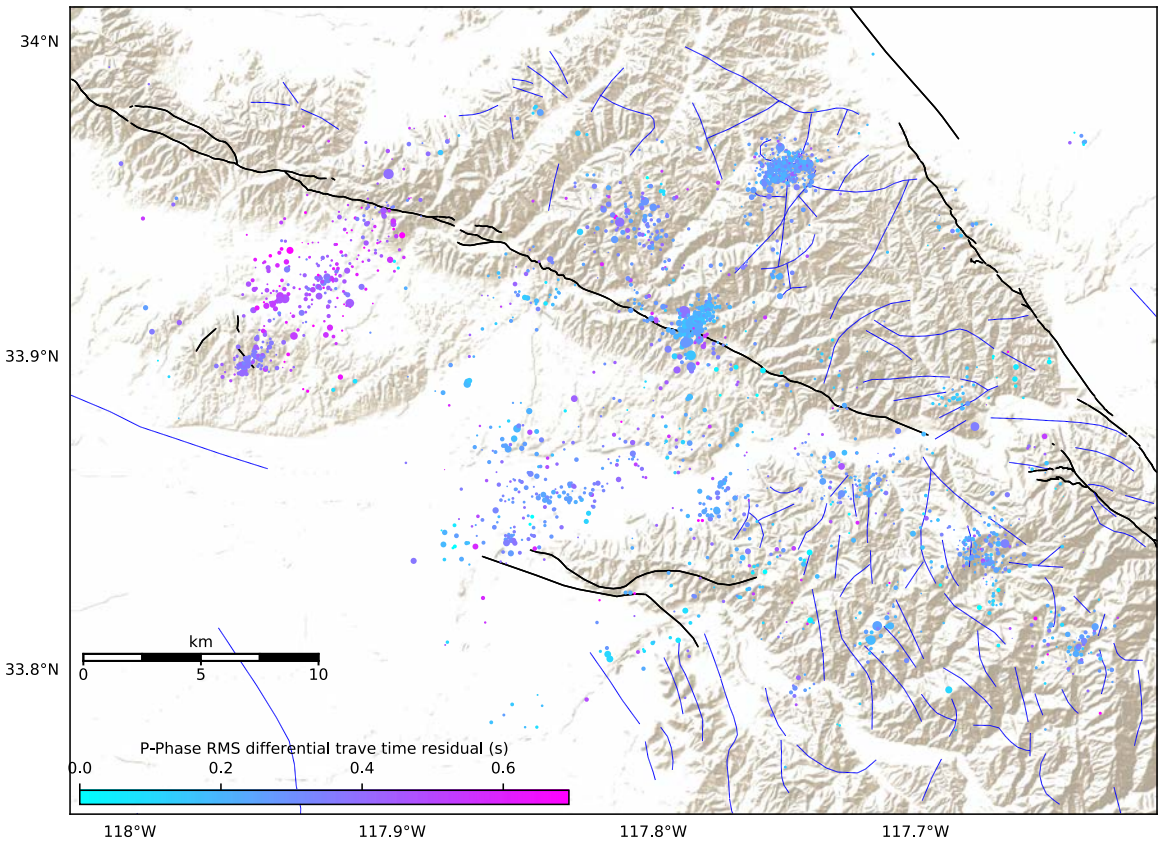

Figure 89: Map of relocated events color coded by their respective RMS residual P-wave differential time from the LA Basin velocity model relocation results under a 0.6 RMS differential travel time residual parameter.

Along with the RMS residual P-waves, the overwhelming majority of the large RMS residual S-wave differential times are also located in the La Habra Sequence (Figure 90). The larger events within the Yorba Linda Sequence still have higher than average RMS residual S-wave differential times. Like the RMS residual P-wave differential times for previous relocation results, nearly all differential times for events comprising the Chino Hills Sequence are low. Figure 91 shows the location errors for these relocation results. Figures 92 and 93 display these location errors based on the location of their events.

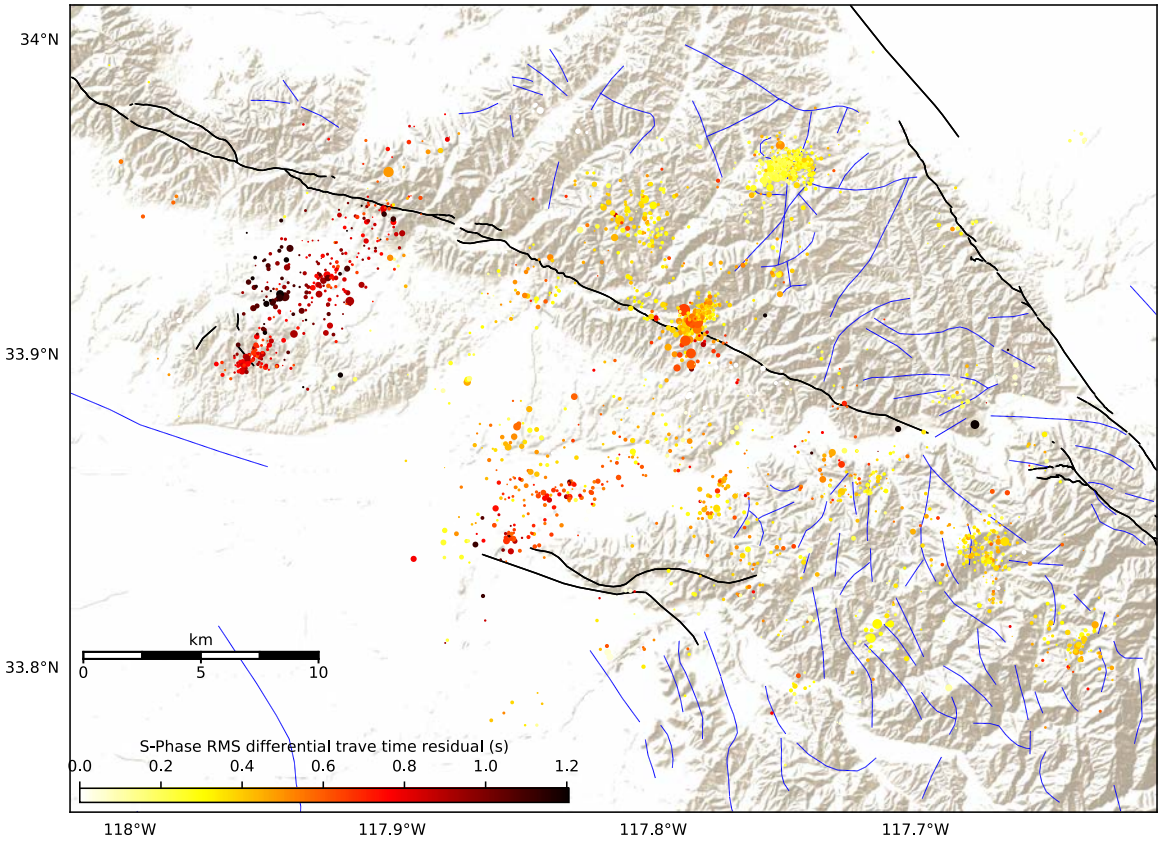

Figure 90: Map of relocated events color coded by their respective RMS residual S-wave differential time from the LA Basin velocity model relocation results under a 0.6 RMS differential travel time residual parameter.

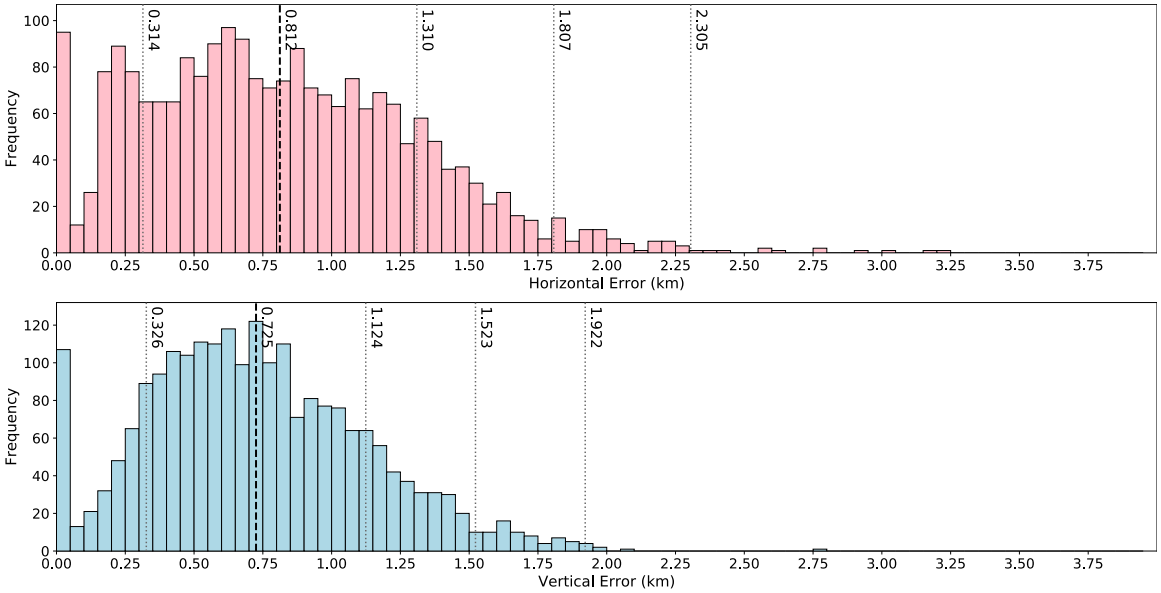

Figure 91: Histograms showing the horizontal and vertical location errors for LA Basin velocity model relocation results under a 0.6 RMS differential travel time residual parameter.

The vast majority of the Yorba Linda Sequence possesses low horizontal location errors, with nearly all of these within Cluster 2 (Figure 92). Contrary to the low horizontal errors of the Yorba Linda Sequence, the vertical errors for are relatively high, particularly those at the northeastern corner of the sequence (Figure 93). Nearly all of the Chino Hills Sequence contain significantly low horizontal errors (Figure 92). These errors are slightly better than the 0.2 RMS LA Basin velocity model relocations, where there were a few earthquakes along the northeastern edge with higher horizontal errors.

For the La Habra Sequence, the location errors of these events correlate with the RMS residual P- and S-wave differential times of the same events (Figure 89, Figure 90). The lower horizontal errors of this sequence are contained within the southwestern events of Cluster 4, while the higher horizontal errors are located towards the middle and northeast segments of the sequence (Figure 92). The vertical errors for this sequence are lower for this sequence as compared to the 0.2 RMS relocation counterparts. As seen with the horizontal errors, the majority of the events with low vertical errors are contained within Cluster 4 at the southwestern edge of the sequence (Figure 93).

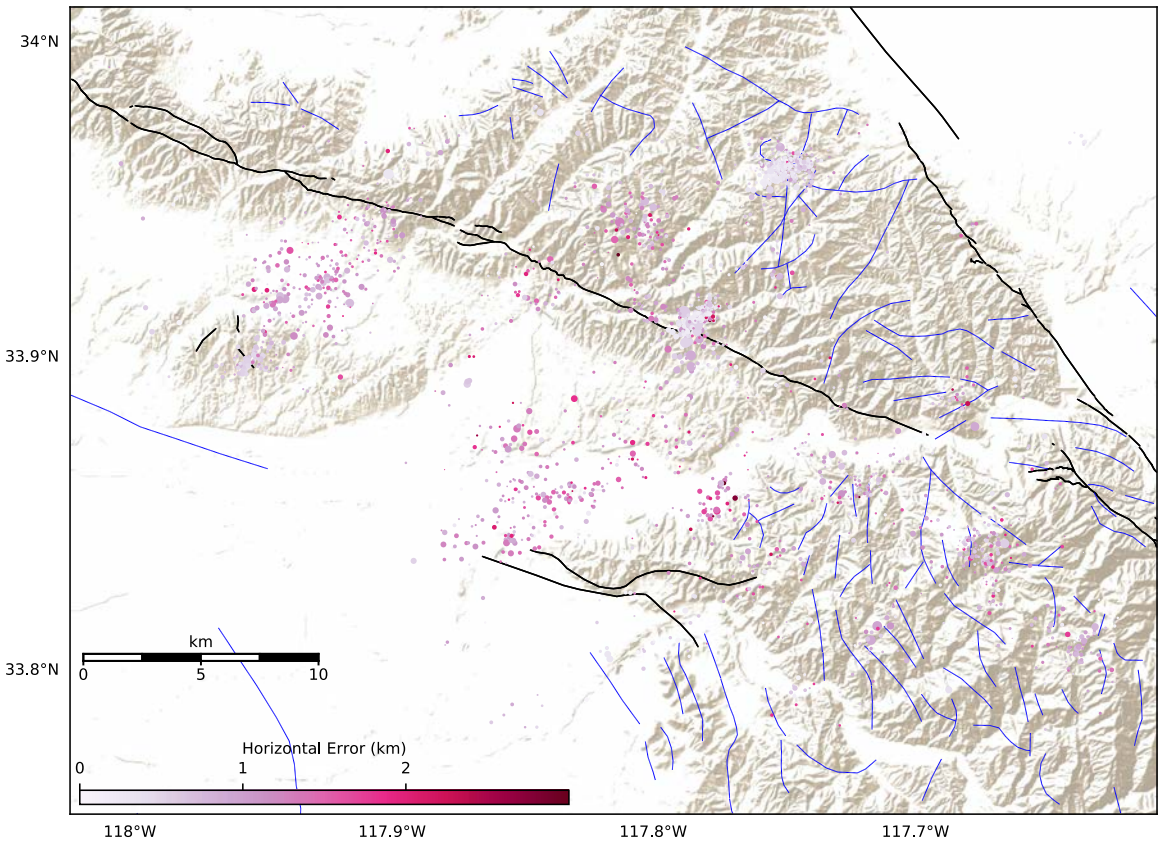

Figure 92: Map of the horizontal errors for of each relocated event using the LA Basin velocity model with a 0.6 RMS differential travel time residual parameter.

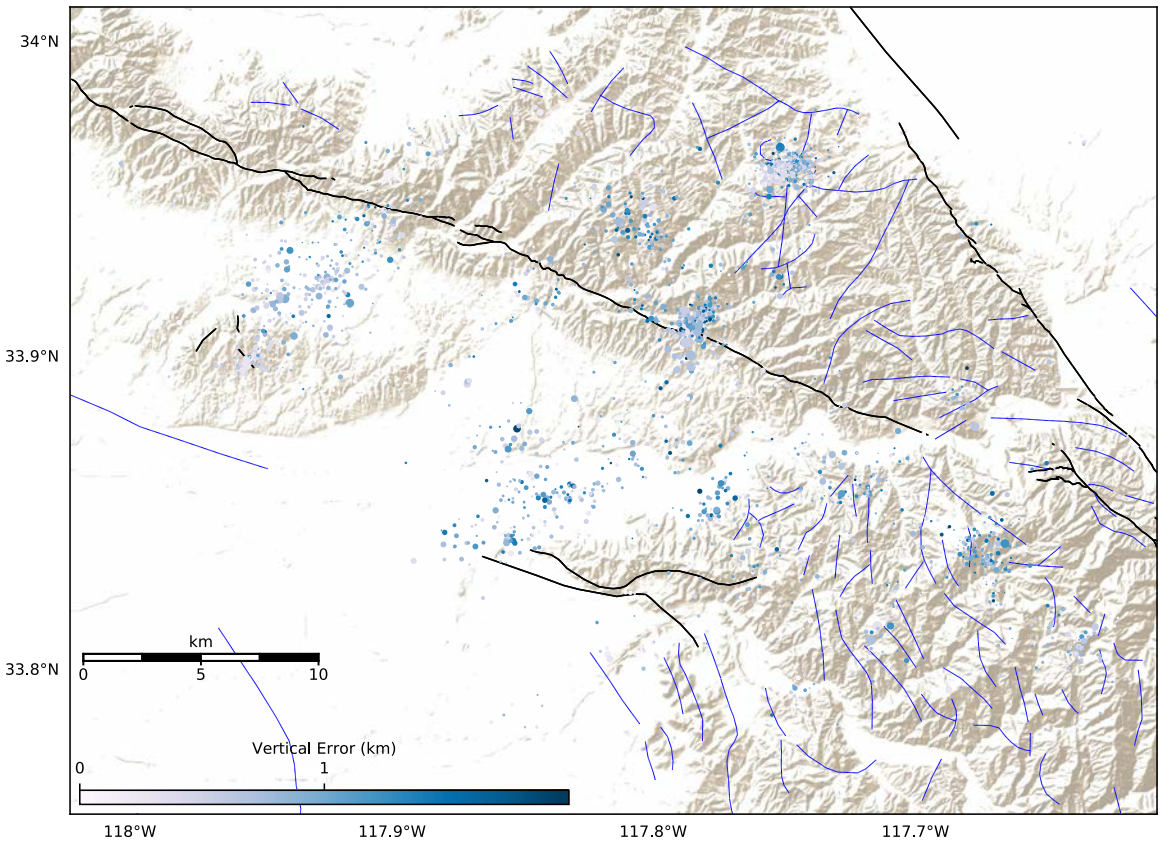

Figure 93: Map of the vertical errors associated with the relocation of events using the LA Basin velocity model with a 0.6 RMS differential travel time residual.

3.2.4 Yorba Linda Sequence Relocation Results for all Velocity Models

The relocations of the Yorba Linda Sequence produced by means of the IASP91 velocity model result in an earthquake trend similar to that seen in prior relocation results (Figure 94-i). When comparing the relocation results produced using the other velocity models for both RMS parameters, this trend of earthquakes is noticeably less consolidated in map view. While the larger events of this sequence do fall within the tight cluster of this sequence, the largest of these events, the M 4.78 earthquake, is offset to the west and occurs at a shallower depth than the remainder of the events (Figure 55-i). The cross section view of this cluster confirms the analysis of the map view in that these relocations are considerably less consolidated than that of the other two model relocations (Figure 95-i).

The relocation results from the utilization of the smoothed southern California velocity model show a tighter consolidation of events than for the IASP91 velocity model (Figure 94-ii). The larger magnitude events, displayed as focal mechanisms, have also aligned along the trend of events, particularly that of the M 4.78 event, which was located towards the west in the IASP91 velocity model relocation results. This event was relocated on the opposite side of the Whittier Fault rather than with the rest of the sequence, implying that the causative fault transects the Whittier Fault. The relocation results of this sequence have oriented themselves into a similar fashion as the prior relocation results; along a trend conjugate to that of the Whittier Fault (Figure 94-ii). These events have a tighter distribution horizontally along a near-vertical trend when observing at depth (Figure 95-ii). The remaining events surrounding the larger two events at shallower depths are part of a separate cluster, as are the deeper events towards the western portion of the cross section (Figure 95-ii).

The relocation results using the LA Basin velocity model have the most consolidated relocations of the three results with a 0.6 RMS differential travel time residual (Figure 94-iii). These relocation results show a higher angle orientation of the trend compared to the other two results, at approximately 75°to the Whittier Fault. The large magnitude events have all situated themselves towards the middle of the sequence, including the M 4.78 event, despite it being adjusted just towards the west. The northeast-southwest nodal plane of the focal mechanisms also correlates well with the overall orientation of the sequence (Figure 94-iii). The other cluster towards the southeast, which possesses shallower events than that of the primary cluster, has been relocated closer to the primary cluster. The cross section of these relocation results confirm that these relocations form a much tighter distribution than those of the other two models (Figure 95-iii).

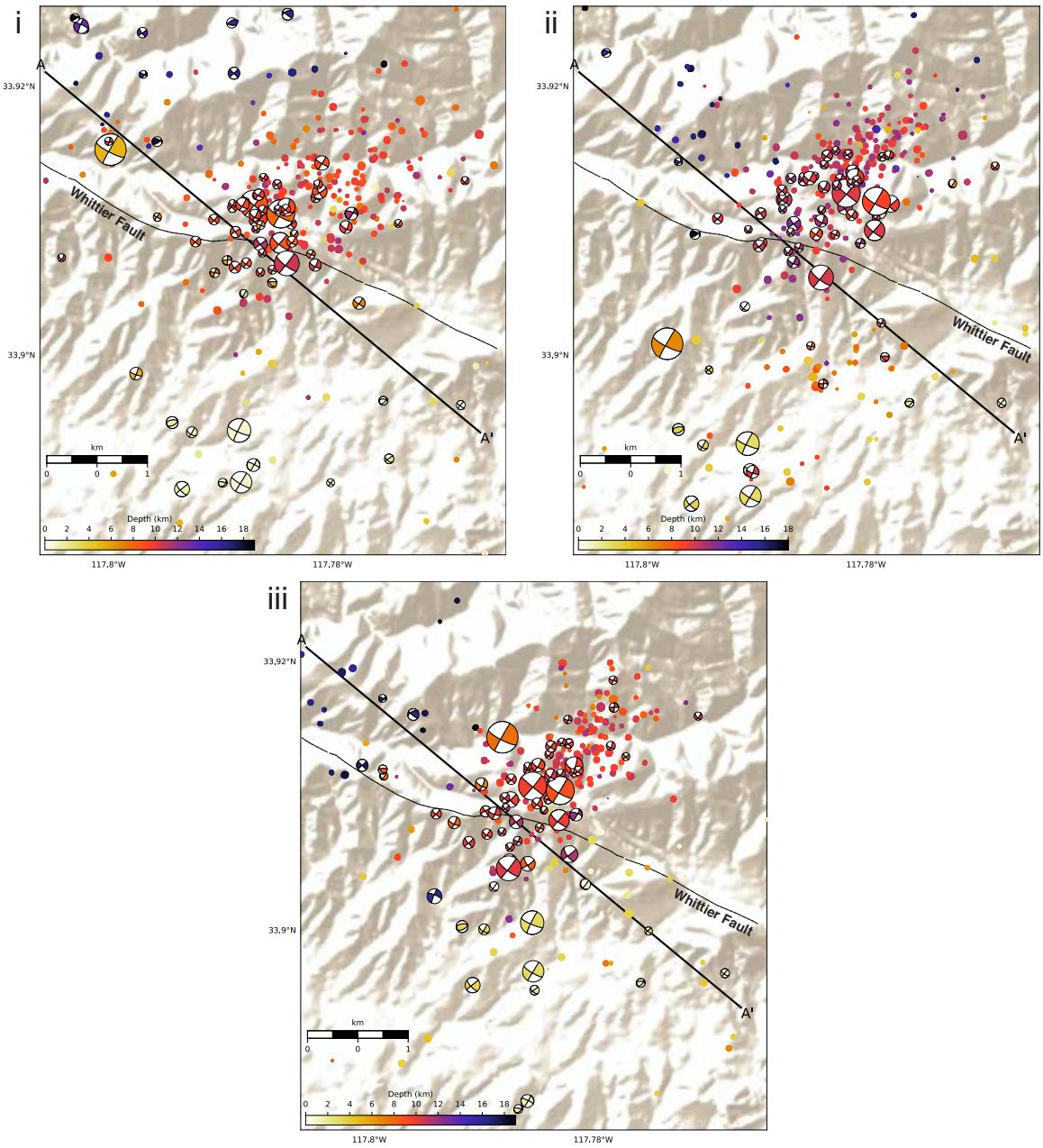

Figure 94: Relocated maps of the Yorba Linda Sequence using a 0.6 RMS differential travel time residual and the three different velocity models. Figure 94-i shows the relocation results using the IASP91 velocity model. Figure 94-ii displays the relocation results using the smoothed southern California velocity model. Figure 94-iii are the relocation results from the LA Basin velocity model. Symbols as in Figure 55.

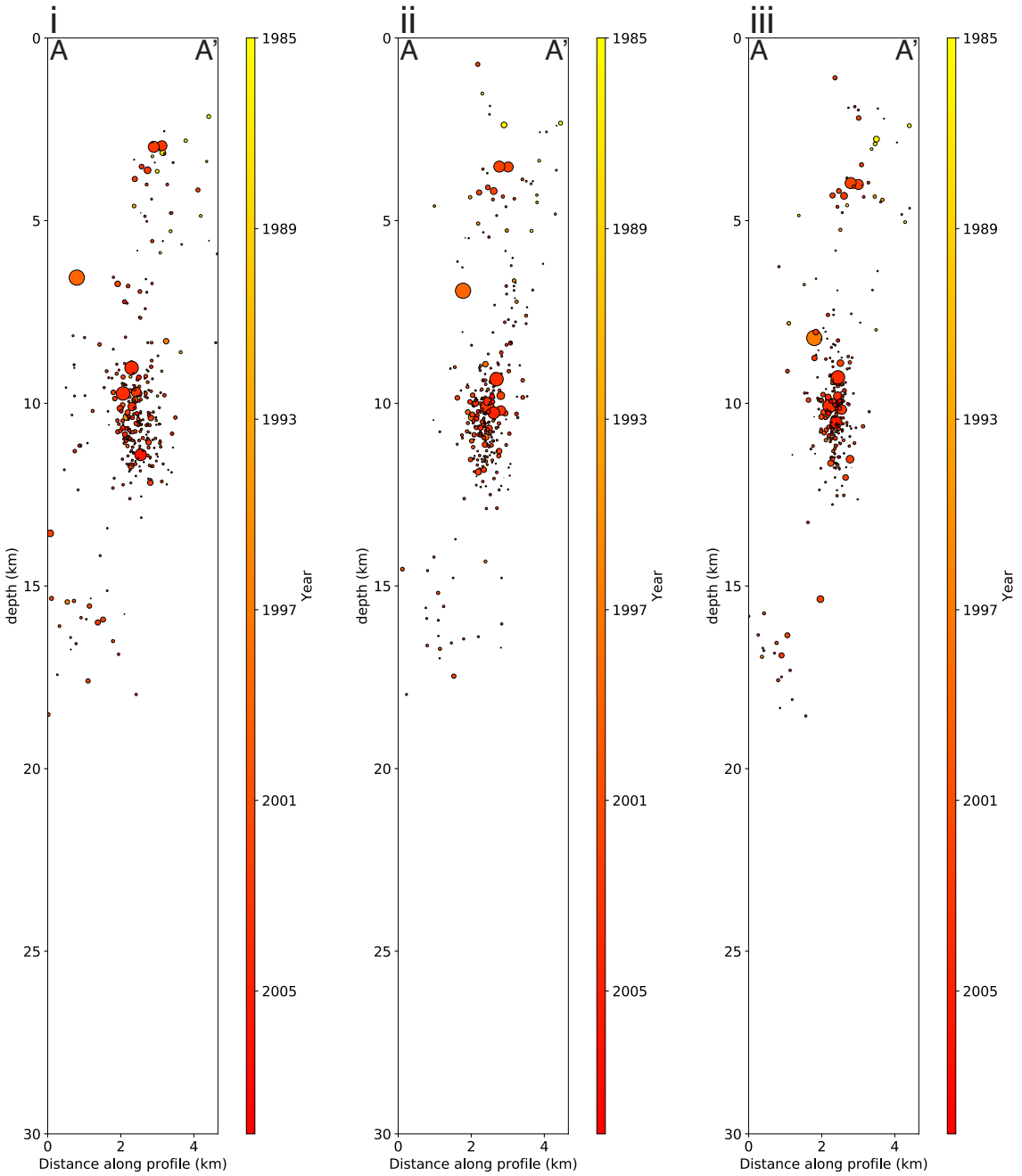

Figure 95: Cross sections illustrating each of the relocations of the Yorba Linda Sequence using a 0.6 RMS differential travel time residual and the three different velocity models. Figure 95-i shows the relocation results using the IASP91 velocity model. Figure 95-ii displays the relocation results using the smoothed southern California velocity model. Figure 95-iii are the relocation results from the LA Basin velocity model.

The location errors of the different relocation results show similar distributions (Figure 96). While the relocation results of the IASP91 velocity model show the least consolidated cluster, the average horizontal error and the spread of errors is the smallest of

the three relocation results (Figure 96-i). Despite having the tightest distribution and the most consolidated relocations, the LA Basin velocity model relocation results have the largest average horizontal error and the widest spread of errors (Figure 96-v).

The vertical errors of each of the relocation results all show a similar distribution of errors (Figure 96). The smoothed southern California velocity model relocation results possess the lowest vertical errors, but have the largest spread of the three results (Figure 96-iv). The average vertical error of these relocation results is 0.705 km. As stated before, while the LA Basin velocity model results have the most consolidated relocations, they possess the largest vertical errors, with an average error of 0.775 km (Figure 96-vi). The IASP91 velocity model relocation results have the smallest spread of the three relocation results (Figure 96-iii).

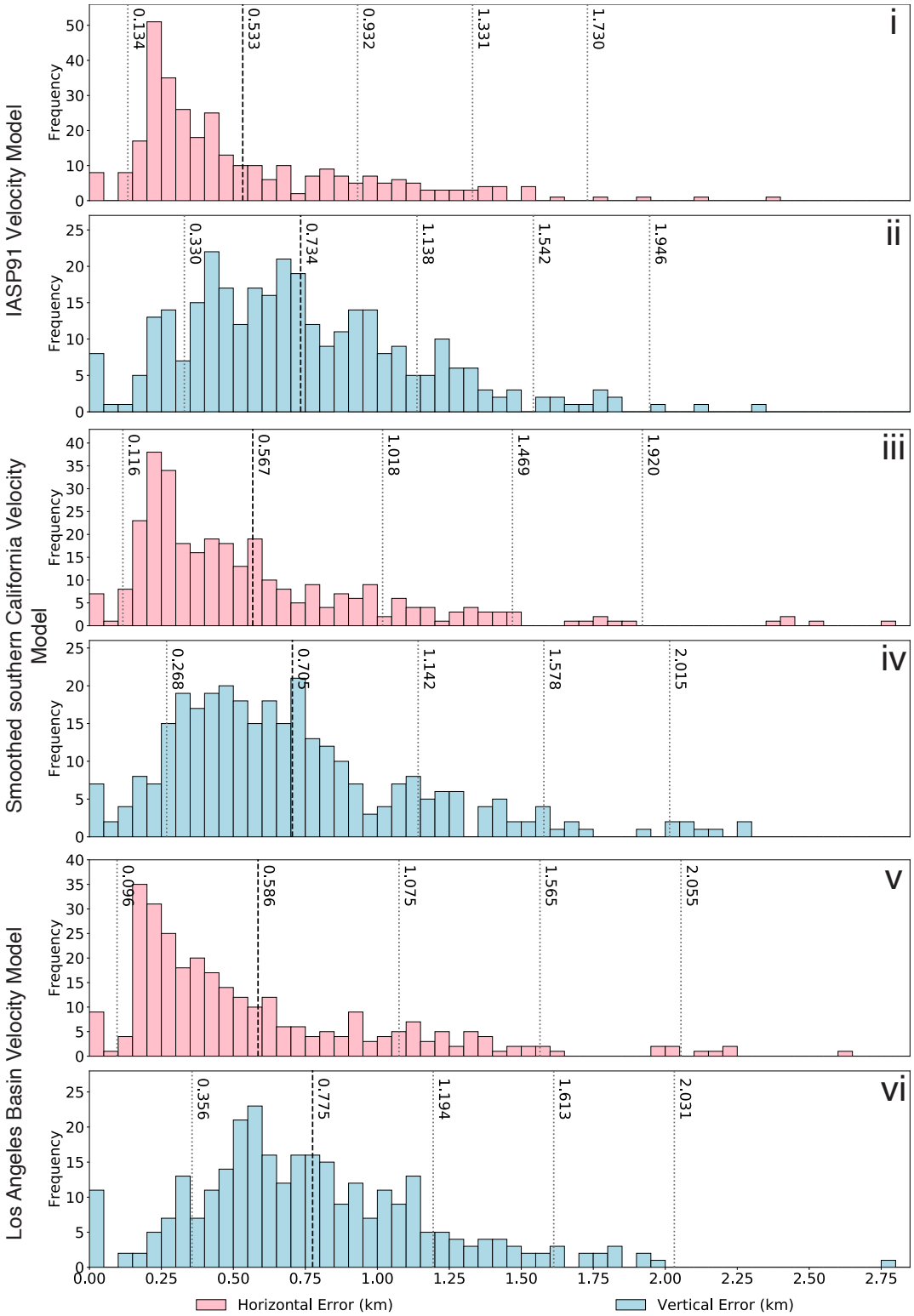

Figure 96: Histograms of the horizontal and vertical errors of the relocations of the Yorba Linda Sequence for each velocity model. The black, dashed line indicates the average location error while the gray, dotted lines denote the standard deviations. Figure 96-i and 96-ii present the errors for the IASP91 velocity model. Figure 96-iii and 96-iv present the errors for the smoothed southern California velocity model. Figure 96-v and 96-vi present the errors for the Whittier Narrows velocity model.

Choosing which of the relocation results is the best for the Yorba Linda Sequence is difficult to confidently determine. All of the relocation results have been consolidated to a northeast-southwest oriented trend, either ceasing at or crossing the Whittier Fault. Visually, the LA Basin velocity model relocation results have the most consolidated distribution, both horizontally and vertically (Figure 94-iii, Figure 95-iii). However, these results have the lowest number of relocated events and the highest horizontal and vertical errors (Figure 96-v, Figure 96-vi). The IASP91 velocity model relocation results have the highest number of relocated events as well as the smallest horizontal errors (Figure 96-i). However, the consolidation of the relocation results is poor among the three relocation results (Figure 94-i). Additionally, the IASP91 velocity model relocations have larger vertical errors than those of the smoothed southern California velocity model relocations, which have the lowest vertical errors of the three (Figure 96-ii).

The northeast-southwest orientation of earthquakes extending from the Whittier Fault indicate a left-lateral fault structure. The northeast-southwest oriented nodal plane of the focal mechanisms of the Yorba Linda Sequence match with this observation. These results compare well with former studies to determine the fault plane of the 2002 Yorba Linda Earthquakes, leading to the conclusion that the events making up the Yorba Linda Sequence most likely situate themselves on a left-lateral conjugate fault to the Whittier Fault (Chen et al., 2005).

3.2.5 Chino Hills Sequence Relocation Results for all Velocity Models

All relocation results for the Chino Hills Sequence have a similar northeast-southwest orientation for this sequence. The consolidation and extent along the trend, however, varies (Figure 97).